PHILOSOPHICAL TRANSACTIONS OF THE ROYAL SOCIETY B BIOLOGICAL SCIENCES

Characterization and Structural Organization of the Organic Matrix of the Radula Teeth of the Chiton Acanthopleura hirtosa

L. A. Evans, D. J. Macey and J. Webb

Phil. Trans. R. Soc. Lond. B 1990 **329**, 87-96
doi: 10.1098/rstb.1990.0153

Characterization and structural organization of the organic matrix of the radula teeth of the chiton *Acanthopleura hirtosa*

L. A. EVANS[1], D. J. MACEY[2]† AND J. WEBB[1]

[1] *School of Mathematical and Physical Sciences and* [2] *School of Biological and Environmental Sciences Murdoch University, Murdoch, Western Australia 6150, Australia*

SUMMARY

The organic matrix of the radula teeth of the chiton *Acanthopleura hirtosa* has been examined by a variety of techniques to identify and partially characterize the major structural component and to elucidate the complex architectural arrangement of matrix fibres. The teeth are initially composed solely of organic material, a major component of which has been identified as the partially deacetylated α-polymorph of the polysaccharide, chitin. The matrix consists of organic fibres, with significant changes in the organization and distribution of fibres occurring in the early stages of tooth development, presumably in preparation for the onset of mineralization. Organic fibres in the posterior region of the tooth cusp become progressively more sparse and poorly ordered. In contrast, the anterior section of the cusp becomes more structured, consisting of a series of highly ordered rope-like fibres. At high magnification these fibres can be seen to consist of hollow tubules linked by fine strands or bridges. Demineralized mature teeth show the same variation in the fibre density and arrangement. It is suggested both that mineralization occurs on a preformed organic framework of which the fibrous bridges are an integral component and that the organization of the matrix fibres together with the architecturally discrete distribution of minerals contributes significantly to the overall mechanical properties of the tooth.

1. INTRODUCTION

Chitons (Mollusca: Polyplacophora) are marine invertebrates that feed by using biominerally hardened teeth to scrape encrusting algae and sponges from the intertidal rocks on which they live (Steneck & Watling 1982). As in all molluscs, the teeth are abraded and broken during feeding and thus need to be replaced on a continuous basis (Runham 1963*a*). Consequently, the radula on which the individual teeth are borne consists of a series of teeth in various stages of development (Webb *et al.* 1989). Initially, the teeth are composed of only a soft organic framework, which is secreted by odontoblast cells at the posterior end of the radula sac (Runham 1963*a*). As the teeth move down the radula, cells of the superior epithelium formed adjacent to the odontoblast cells move with them (Runham 1963*a*) and are intimately involved in the deposition of the various minerals involved in biomineralization (Kim *et al.* 1989). Although all chiton radulae have 17 teeth per row, only 2 teeth, the major laterals, are directly responsible for abrading the substratum (Steneck & Watling 1982). The major laterals become impregnated with several iron biominerals starting with ferrihydrite ($5Fe_2O_3 \cdot 9H_2O$). At later stages magnetite (Fe_3O_4), lepidocrocite (γ-FeO·OH) and goethite (α-FeO·OH) are the major iron biominerals present (Webb *et al.* 1989). The major lateral teeth also contain calcium, generally as apatite ($Ca_5OH(PO_4)_3$) or an apatite-like material (Lowenstam 1967; Lowenstam & Weiner 1985; Kim *et al.* 1986). Mineral deposition within the tooth cusp is very site specific, and by the time the teeth are approaching maturity each of the various minerals is found in architecturally discrete compartments (Lowenstam 1967).

The organic framework that initially makes up the tooth is composed of the polysaccharide chitin, with various proteinaceous components (Runham 1963*b*). Chitin is well known from other animal groups, and while it consists of β-(1→4)-linked 2-acetamido-2-deoxy-D-glucose residues, it is normally associated with large amounts of protein and thus can be considered a glycoprotein (Muzzarelli 1973). Because of the rigidity of the chitin macromolecule, it is often called a support polysaccharide (Furth 1980) a role demonstrated in the cuticle of arthropods (Barnes 1980). Three crystalline forms of chitin have been identified by X-ray diffraction (Rudall 1963). By far the most common is α-chitin, which consists of an array of anti-parallel hydrogen-bonded chains. By contrast, β-chitin, has parallel chains, whereas in γ-chitin (the rarest form) there are two chains 'up' (parallel) to every one 'down' (anti-parallel) (Muzzarelli 1977).

Although several studies have detailed the structure of the fully formed tooth (see, for example, Lowenstam (1967); Kim *et al.* 1989) very little information is

† To whom correspondence should be addressed.

available about the structure of the organic matrix associated with the mineral deposits. Our study was thus initiated to characterize more fully the chemical nature and the anatomy of the organic matrix of the major lateral teeth in the chiton *Acanthopleura hirtosa*. Techniques used included chemical analysis, light microscopy and scanning and transmission electron microscopy. A detailed knowledge of the structure of the matrix on which mineralization occurs is essential if progress is to be made in both elucidating the way in which this complex biomineralization process is controlled and how the organic matrix contributes to the overall mechanical properties of the tooth.

2. MATERIALS AND METHODS

Specimens of *Acanthopleura hirtosa* were collected near the Perth metropolitan area (latitude 32° S, longitude 116° E). Radulae were cut into segments according to developmental stages of tooth maturation as given by Kirschvink & Lowenstam (1979). In our study stages 1 and 4 were used for analysis. Immature segments of chiton radula (stage 1) were used for light microscopy and for the determination of the polysaccharide phase present, as the presence of mineral forms interferes with histochemical staining techniques, infrared spectroscopy and X-ray diffraction analyses. Fully mature segments (stage 4) were used for further light and electron microscopy.

For identification of chitin by Fourier-transform infrared spectroscopy (FT–IR) stage 1 segments were deproteinated with boiling dilute alkali, repeatedly washed with distilled water and dried exhaustively at 78 °C under vacuum. β-chitin used as a reference standard was obtained from squid pens by removing the protein and drying as for radula chitin. Crab carapace α-chitin was obtained from Sigma Chemical Company. Some of this practical grade powder was also purified according to the method of Skujins *et al.* (1965). As this method involves treatment with cold concentrated hydrochloric acid, squid pen chitin could not be purified by this method because it will convert to the more stable α-form (Walton & Blackwell 1973). No appreciable differences were found between spectra of crab chitin samples that had been purified and those that had not. KBr discs were prepared for each sample type by mixing approximately 5 mg of sample with 200 mg KBr (BDH, Analar grade) and grinding in a Specac vibrator mill. Pellets (12 mm) were formed by using an evacuable die; FT–IR spectra were recorded by using a Perkin Elmer 1720-X spectrometer.

For powder X-ray diffraction analysis (XRD), similar radula samples were deproteinated and dried as for FT–IR, then ground as finely as possible using an agate vibrator mill before being placed onto low background quartz plates using a liquid gum fixative (Gibson Chemicals). Samples of crab α-chitin and squid pen β-chitin were prepared in the same manner. Analysis was done with a Philips PW1700 automated powder diffractometer controlled by a PDP-11 microcomputer. The X-ray source was CuK_α radiation generated by a PW1729 X-ray generator running at 40 mA and 45 kV. The system used an automatic divergence slit with a step scan of 0.025° s^{-1}. Diffraction patterns were recorded in the peak angle 2–70° and plotted on a Philips PM8154 plotter.

For histochemical examination, some segments were fixed overnight in glutaraldehyde (3% by volume) in seawater then treated for 24 h with boiling dilute alkali to remove the protein. Other segments were placed in seawater only, deproteinated only or fixed in glutaraldehyde only. All segments were then dehydrated, embedded in paraffin wax and sectioned at 5 μm. Periodic acid/Schiff's (PAS) staining was done according to McManus (1946). To ensure that any positive reaction was not due to residual glutaraldehyde, segments were treated with appropriate blocking agents (dimedone or dinitrophenylhydrazine (DNPH)). Alcian blue and Hale's colloidal iron techniques were done according to Culling (1974). To differentiate between acidic and neutral mucopolysaccharides, a combined PAS – Alcian blue method was also employed (Culling 1974). Van Wisselingh's test was done on radular segments that had been converted to chitosan (Tracey 1955). A suitable control material was included for each staining technique to check the reliability of the procedure.

For light microscopy stage 1 segments were fixed in 70% ethanol, dehydrated by using absolute ethanol followed by toluene, infiltrated for 4 days at 4 °C with methyl methacrylate solution and finally polymerized in fresh infiltration solution for 4 days at 32 °C in an oxygen-free environment. Blocks were sectioned by a tungsten carbide knife on a Reichert-Jung 2050 microtome. After removal of the resin with warm xylene, sectioned material was stained with methylene blue – azure II in borax solution (Richardson *et al.* 1960).

For scanning electron microscopy (SEM) stage 4 radular segments were cleaned briefly with NaOCl (30 g l^{-1}), fixed in a solution of glutaraldehyde (3% by volume) in seawater for approximately 6 h, rinsed with seawater and then demineralized for 24 h with 4 M HCl at 37 °C. Other segments were fixed with glutaraldehyde, cleaned in 1 M NaOH according to the method of Van der Wal *et al.* (1989) and then demineralized with HCl as above. All segments thus treated were dehydrated through a graded series of alcohols, dried at the critical point of carbon dioxide, mounted on aluminium stubs and coated with a thin layer of carbon followed by gold. Yet other radular segments, with the mineral left intact, were fixed in glutaraldehyde, cleaned in NaOCl (30 g l^{-1}), air dried, and then crushed gently with a boron carbide mortar and pestle to fracture the tooth surfaces. These segments were then mounted on stubs and carbon and gold coated. Specimens were viewed on a Philips 501B scanning electron microscope.

For transmission electron microscopy (TEM) radular segments were fixed and demineralized as for SEM. Specimens were then dehydrated through a graded series of alcohols, transferred to propylene oxide and infiltrated with an Epon–Araldite mixture by introducing the resin gradually over 5 days. Ultrathin sections were cut at 60–70 nm by using glass knives on a Reichert-Jung OmU3 ultramicrotome, treated with

PHILOSOPHICAL TRANSACTIONS OF THE ROYAL SOCIETY B BIOLOGICAL SCIENCES

saturated aqueous uranyl acetate and lead citrate (Reynolds 1963) and placed on 200 mesh copper grids. Radular sections were viewed using a Philips 301 electron microscope.

3. RESULTS

Identification of chitin

FT–IR

The FT–IR spectrum of deproteinated stage 1 chiton radula closely matched those of the standard material obtained from crab carapace and squid pen, indicating that chitin is a major component of the radula organic matrix (figure 1). However, the stage 1 spectrum was less well defined than the infrared spectra of the two standards.

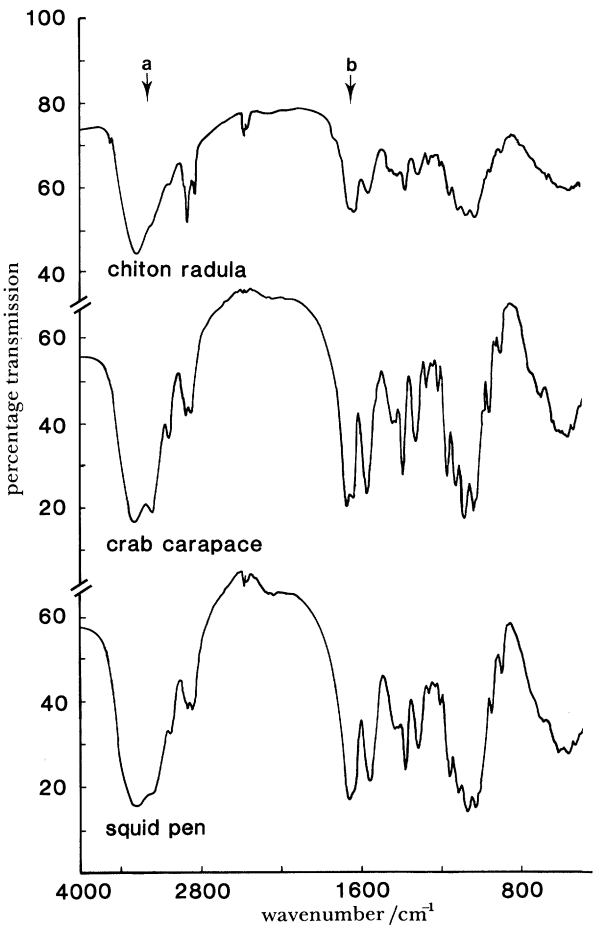

Figure 1. Fourier-Transform infrared spectra obtained from chiton radula, crab carapace (α-chitin) and squid pen (β-chitin) showing percentage transmission versus wavenumber (a) N—H region; (b) C=O region.

In all spectra, a strong band at about 3440 cm^{-1} was assigned to an OH stretching vibration, whereas that in the 3300–3260 cm^{-1} region was due to NH stretching vibrations. Although the OH and NH peaks are well separated in the crab (α-chitin) spectrum, these two peaks were less clearly resolved in the chiton and squid (β-chitin) spectra despite exhaustive drying procedures.

Bands occurring between 1660 and 1620 cm^{-1} were due to C=O stretching vibrations (amide 1 band). In the spectrum of squid pen chitin, poorly resolved bands were apparent at about 1646 cm^{-1}, whereas for both radular chitin and crab carapace chitin, these bands were clearly resolved. The relative intensities of these two bands were reversed, however, for chiton radula compared with crab and squid. The amide II band occurred at almost exactly the same wavelength for all forms of chitin investigated (1556 cm^{-1}). Broad bands occurring just below 3000 cm^{-1} were assigned to CH stretching vibrations with CH bending vibrations occurring at much lower frequencies (around 1450 cm^{-1} and 1375 cm^{-1}). The two low intensity bands occurring at about 2360 and 2344 cm^{-1} are due to atmospheric CO_2.

All spectra showed several strong bands in the 1250–950 cm^{-1} region, which can be attributed to the CO (single bond) linkages occurring in the chitin molecule, such as the C—O—C and C—OH groups occurring in the ring structure, and the glucosidic C—O—C linkage (Darmon & Rudall 1950).

XRD

XRD data obtained from stage 1 segments of *A. hirtosa* radula indicated that the first d-spacing occurred in the 9.5–10 Å† range as did that of the crab carapace α-chitin (table 1). In contrast, squid pen β-chitin gave a major spacing well above 10 Å. This is a conclusive indication that radular chitin is present as the α-form as only α-chitin will give the first major spacing between 9.5 and 10 Å, with the β-form giving a characteristic d-spacing of approximately 11 Å (Muzzarelli 1973; Gow *et al.* 1987). Several other reflections were shared by all three samples. Diffraction patterns from chiton radula and squid pen were generally more diffuse than those obtained from crab carapace.

Table 1. *XRD data*

(Data show angle of diffraction, 2θ; planar spacings, d (in ångstroms); with their observed intensities, I_0, for material obtained from chiton radula, squid pen and crab carapace. Note observed intensities were estimated as very strong, VS; strong, S; moderately strong, MS; medium, M; weak, W; or very weak, VW.)

chiton radula			crab carapace α-chitin			squid pen β-chitin		
2θ deg.	d Å	I_0	2θ deg.	d Å	I_0	2θ deg.	d Å	I_0
8.96	9.87	S	9.26	9.55	S	8.21	10.77	S
12.85	6.89	VW	12.68	6.98	W	—	—	—
19.24	4.61	VS	19.20	4.62	VS	19.76	4.49	VS
—	—	—	20.77	4.28	MS	—	—	—
—	—	—	23.35	3.81	M	—	—	—
26.67	3.34	S	26.40	3.37	M	26.66	3.34	MS
—	—	—	32.08	2.78	VW	28.23	3.16	W
—	—	—	34.94	2.57	VW	—	—	—
39.06	2.23	VW	38.35	2.35	W	—	—	—
42.53	2.12	VW	—	—	—	—	—	—
49.83	1.83	VW	—	—	—	—	—	—
54.86	1.67	VW	—	—	—	—	—	—

Histological staining techniques

The staining reactions for stage 1 tooth cusps from *A. hirtosa* are summarized in table 2. Van Wisselingh's (chitosan) test gave a positive reaction, which con-

† 1 Å = 10^{-10} m = 10^{-1} nm.

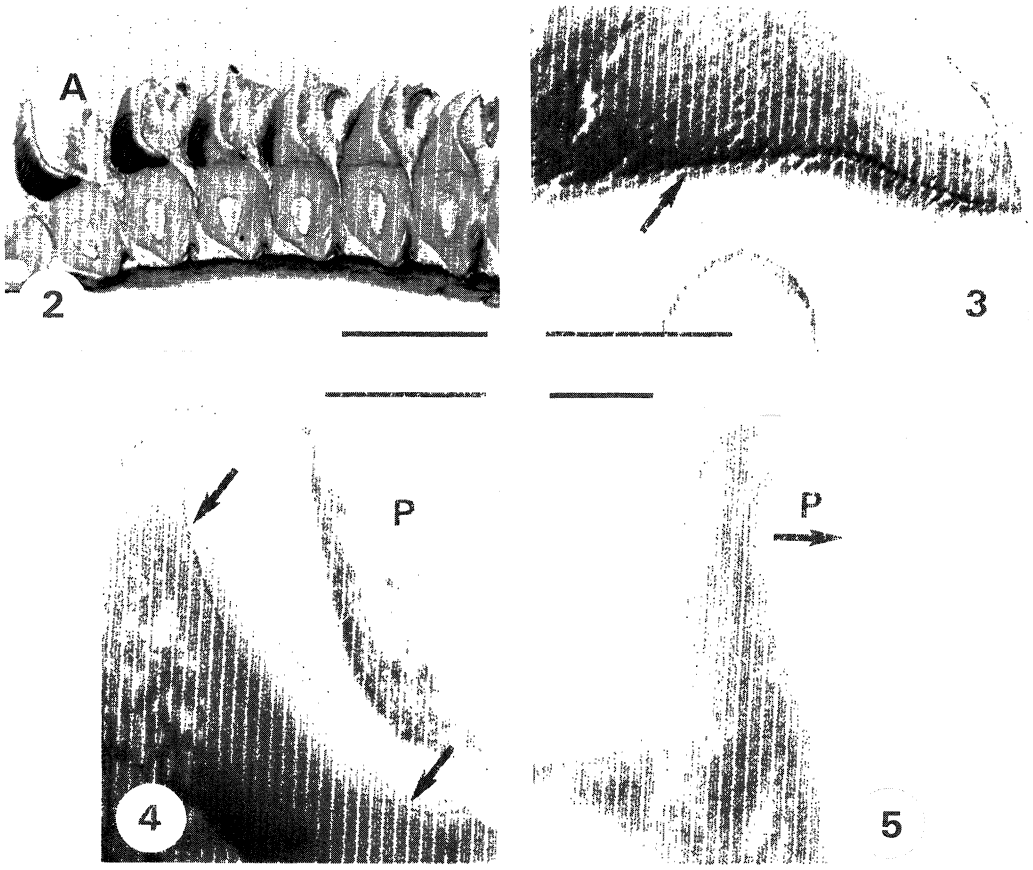

Figure 2. Light micrograph (LM) of longitudinal section through the major lateral teeth following initial tooth formation (stage 1) stained with methylene blue – azure II. Most mature teeth are denoted by A. Scale bar 500 μm.

Figure 3. LM of longitudinal section of major lateral tooth at row 8 showing double-layered junction zone (arrow). Scale bar 50 μm.

Figure 4. LM section of a demineralized mature cusp (stage 4) showing the presence of a line (arrows) delineating anterior and posterior regions of the cusp. P indicates posterior surface of the cusp. Stained with Toluidine blue. Scale bar 100 μm.

Figure 5. LM section of an immature tooth cusp (stage 1) stained using Van Wisselingh's technique for chitosan and revealing the presence of a dense network of fibres. P indicates posterior surface of the cusp. Scale bar 50 μm.

Table 2. *Histochemical reactions of stage* 1 *chiton radula*

(Stains used were: Periodic Acid/Schiffs reagent, PAS, both with and without dimedone or dinitrophenylhydrazine as blocking agents; Alcian blue, Ab; Hales colloidal iron, Hales and the Van Wisselingh staining test for chitosan. Note, the latter test requires treatment with saturated KOH at 160 °C before staining and thus the first three categories of treatment are not applicable. Full details of fixation and staining can be found in the text.)

	treatment			
method	untreated	fixed	deproteinated	fixed/ deproteinated
PAS	weak + ve	strong + ve	weak + ve	weak + ve
PAS (with blocking agent)	weak + ve	weak + ve	− ve	− ve
Alcian blue	weak + ve	weak + ve	+ ve	+ ve
PAS/Alcian blue	some weak PAS + ve/ Ab − ve	PAS strongly + ve/some Ab + ve	PAS − ve/some Ab + ve	PAS − ve/some Ab + ve
Hale's	Bases + ve	strongly + ve	+ ve	+ ve
Van Wisselingh	—	—	—	+ ve

firmed the presence of chitin in these teeth (table 2). Only chitin would have been present as this method requires harsh treatment with KOH to effect the conversion of chitin to chitosan and thus any protein present as a component of the organic matrix would have been removed.

Hale's colloidal iron method showed a weak positive reaction in the cusps, which decreased in intensity

towards the anterior end of the radula. This was the case for both fixed only, and fixed and deproteinated teeth, although the latter did not stain as strongly as those in which the protein remained. Alcian blue gave a weak staining reaction, but staining intensity increased in all teeth once the protein had been removed.

A positive reaction with PAS staining was obtained only in the absence of blocking agent or when the teeth had not been deproteinated. Sections that had the protein removed and had been treated with either dimedone or DNPH before staining showed no reaction. The combined PAS – Alcian blue technique confirmed that PAS staining is due to the presence of protein, as specimens that were fixed only were PAS positive whereas those that were deproteinated were negative. Some Alcian blue staining was observed in both cases.

Organization of organic fibres

Light microscopy

Sections through the first two rows of stage 1 teeth stained with methylene blue – azure II showed both cusp and base in these very young teeth to be generally fibrous in nature, with the junction zone, which separates the cusp and base, appearing as a faint line. Over approximately the next five tooth rows a gradual decrease in staining intensity occurred in the posterior region of the tooth cusp, resulting in the development of a clear area (figure 2). This was followed in turn by the development of an intense staining reaction at the anterior surface which eventually occupied the entire anterior region of the cusp (figure 2). The junction zone showed a concomitant sequential development, appearing as a highly pronounced double-layered structure by row 8 (figure 3). Under polarized light a dark band separating anterior and posterior regions was also observed at this stage. Sections of acid-treated fully mature teeth (stage 4) viewed under normal light showed a similar distinct band separating the anterior and posterior cusp regions. This appeared as a thin golden-brown line which also extended part-way down the anterior surface (figure 4).

Sections of individual stage 1 teeth in which the chitin had been converted to chitosan revealed the presence of a dense network of fibres running through the cusp (figure 5). At least two major ridges of fibres were evident extending from the lower region of the cusp and running up towards its apex, parallel to anterior and posterior cusp surfaces, respectively (figure 5). Finer fibres emerged from the major anterior chitin ridge, curving round to lie almost perpendicular to the anterior cusp surface. These fibres were less apparent towards the posterior side of the cusp. Fibre density, as evidenced by increased staining intensity, was greatest in the lower regions of the cusp.

SEM

SEM of fractured fully mineralized (stage 4) teeth showed that fracturing usually occurred across the posterior surface of the cusp well above the junction zone. At this point a discrete layer of mineral, approximately 15 μm thick and presumably corresponding to the magnetite layer, was evident (figure 6). Many densely packed vertical fibres were observed behind the magnetite layer (figure 6).

Cleaning of the major lateral teeth with hot alkali followed by acid etching removed a major portion of the posterior region of the cusp, again revealing the presence of vertical rope-like strands of material, presumably chitin (figure 7). These strands originate in the lower section of the cusp, where they occupy the full width, before rising and curving back towards the anterior surface (figure 8). A horizontal discontinuity was observed on the posterior surface approximately 35 μm above the junction zone (figure 9) which possibly corresponds to the edge of the region of magnetite deposition. The thickness of this discontinuity varied across the width of the tooth, but usually did not exceed 15 μm.

In marked contrast, specimens that had been hypochlorite-cleaned and acid-treated, showed etching of only the surface layers of the posterior tooth cusp (figure 10). This less vigorous treatment of the teeth revealed the presence of polygonal tubules beneath the posterior tooth surface (figure 11). The surface covering of the teeth seemed more resistant to this treatment than the cusp interior, often remaining relatively intact. When surface etching did occur, it took place in the lower regions of the cusp, leaving the surface covering at the tip of the cusp untouched (figures 10 and 11).

TEM

Significant differences were seen between different regions of the organic matrix in mature tooth cusps that had been extensively demineralized by acid treatment. Examination of the posterior region of the tooth cusp, from which the magnetite had been removed, revealed the presence of poorly ordered fine organic fibres (figure 12). In contrast, the anterior region of the cusp (that is, the apatite-bearing compartment) contained fibres that were highly organized, appearing as long hollow tubules approximately 0.15–0.20 μm in diameter (figures 13 and 14). These tubules appeared to be interconnected by an organic network of finer fibrils. In longitudinal sections, some interconnecting fibrils were seen as thicker strands or bridges making an angle of between 30 and 50° with the major axis of the tubules (figure 15). The contrast between the two types of organic matrix was seen most clearly at the junction between the anterior and posterior regions (figure 16). In addition, the boundary line which appeared golden-brown under the light microscope was evident as a diffuse line of crystallites bordering the magnetite-bearing compartment (figure 16).

Some mineral content always remained in other specific locations, despite the acid treatment. For example, both acicular and cuboidal crystals were seen along the anterior surface, with needle-like crystals aligning themselves along the fibrous bridges (figure 15). Along the posterior surface, a few crystals were seen (figure 17).

PHILOSOPHICAL TRANSACTIONS OF THE ROYAL SOCIETY B BIOLOGICAL SCIENCES

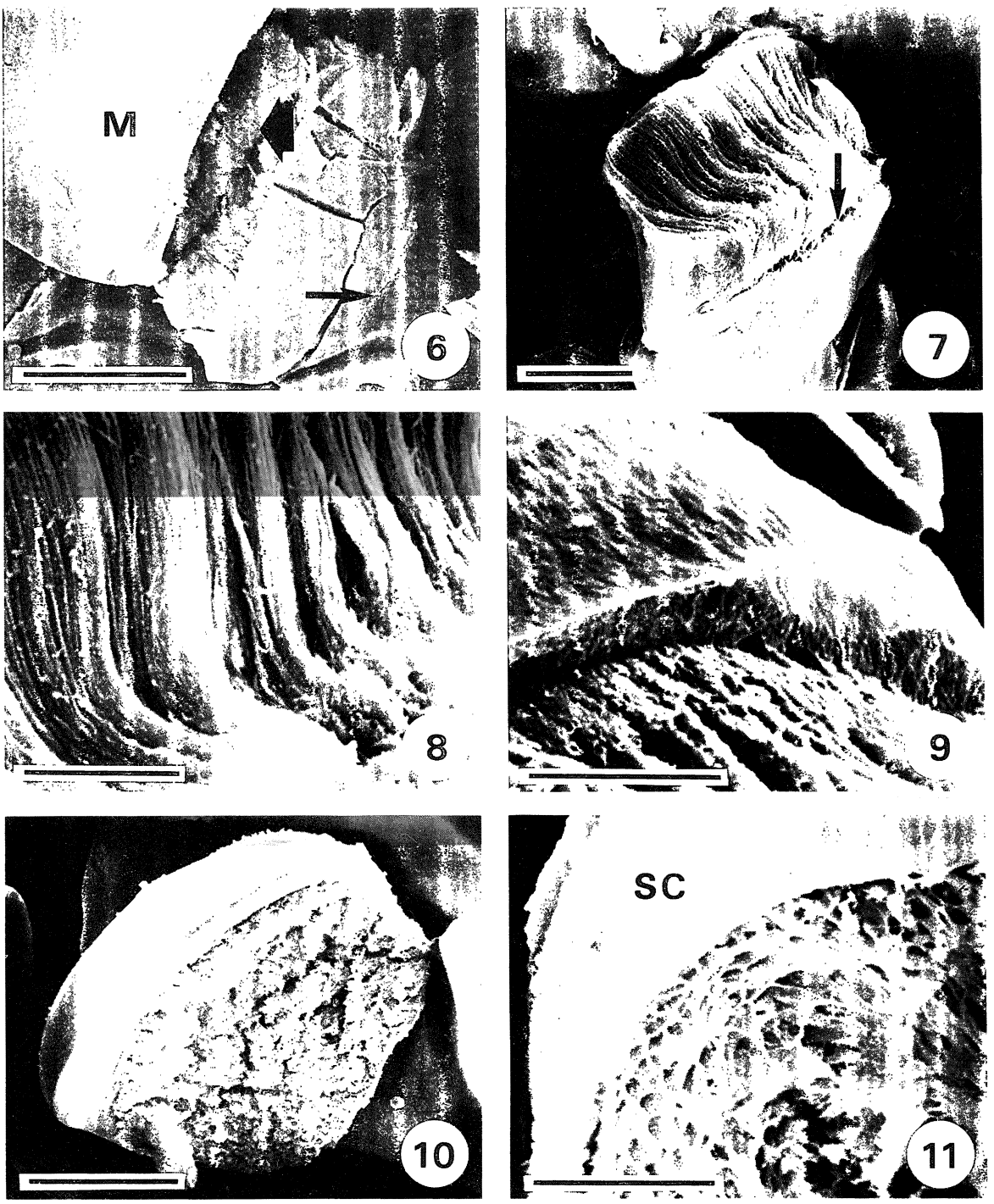

Figure 6. SEM of the posterior surface of a fractured fully mature (stage 4) tooth revealing the presence of a discrete mineral layer, presumably magnetite (M) in front of densely packed vertical fibres (broad arrow). The junction zone (thin arrow) is also visible well below the major fracture line. Scale bar 100 μm.

Figure 7. SEM of an alkali-cleaned acid-etched tooth cusp viewed from the posterior surface showing the presence of vertical rope-like strands of material, presumably chitin. Note, all of the posterior region of the cusp together with parts of the anterior region have been removed during processing. A prominent discontinuity is apparent on the posterior surface (arrow) above the junction zone. Scale bar 50 μm.

Figure 8. Higher-powered SEM of the same tooth as in figure 7 showing the detailed structure of the rope-like strands of chitin. Scale bar 25 μm.

Figure 9. SEM of the horizontal discontinuity frequently observed in alkali-cleaned acid-etched teeth corresponding to that arrowed in figure 7. Scale bar 25 μm.

Figure 10. SEM of the posterior surface of a hypochlorite-cleaned acid-etched tooth showing removal of only the surface layers. Scale bar 100 μm.

Figure 11. SEM of a hypochlorite-cleaned and more deeply acid-etched tooth showing the presence of polygonal tubules beneath the posterior tooth surface. Note surface covering (SC) still remains near the tip of the cusp. Scale bar 25 μm.

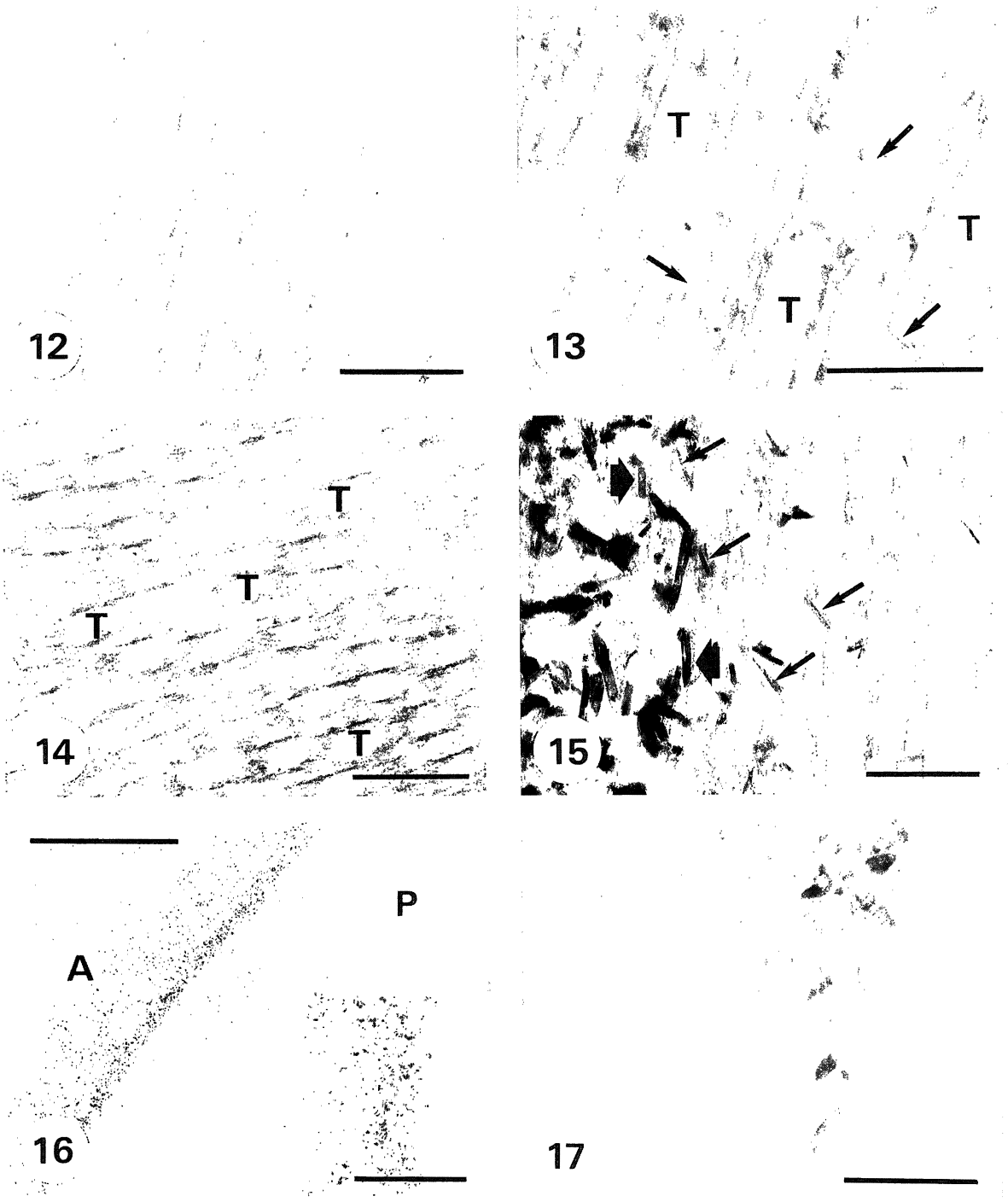

Figure 12. TEM of a stained section of an area of the organic matrix in the posterior region of an acid-treated (stage 4) tooth cusp showing the presence of sparse fibres. Scale bar 0.5 μm.

Figure 13. TEM of a stained longitudinal section of the anterior region of an acid-treated tooth cusp showing the presence of highly organized fibres arranged as hollow tubules. In some cases cross-links (arrows) can be seen between the tubules (T). Scale bar 0.5 μm.

Figure 14. TEM of a stained transverse section of a similar area to that shown in figure 13. The hollow tubules are now apparent as interconnected open rings (T). Note the contrast in fibre density between figure 12 (posterior region) and figures 13 and 14 (anterior region). Scale bar 0.5 μm.

Figure 15. TEM of a stained longitudinal section of the anterior region of an acid-treated mature tooth near the surface. In this region some mineral crystals still remain oriented both parallel to the long axis of the tubules (broad arrows) and along the interconnecting fibrous bridges (fine arrows). Scale bar 0.5 μm.

Figure 16. TEM of a stained section of the junction between the posterior (P) and anterior (A) regions of an acid-treated mature cusp showing a diffuse line of crystallites along the boundary line. Scale bar 10 μm. Inset: higher-power TEM of boundary crystallites. Scale bar 2 μm.

Figure 17. TEM of a stained section of the posterior cusp surface of an acid-treated mature cusp showing the more complex orientation of the fibres at the surface together with the presence of a few crystals. Scale bar 0.5 μm.

4. DISCUSSION

This study has shown that chitin within the major lateral teeth of chitons is laid down in a complex arrangement that almost certainly dictates the morphology of the final tooth structure. In addition, it has confirmed previous studies suggesting that chitin comprises a major component of the organic matrix of chiton teeth and has conclusively identified the crystallographic form of chitin as the α-form.

Both FT–IR and XRD indicated that chitin is the product remaining after stage 1 segments have been treated to remove protein. However, radular chitin spectra showed a decrease in sharpness of infrared absorption bands compared with those obtained for squid pen and crab carapace, reflecting a decrease in order within the chitin macrostructure of stage 1 segments. Similarly, diffraction patterns obtained from radular chitin indicated that this chitin is poorly crystalline. In the infrared spectrum of chitin, the two main areas of interest at 3300–3260 cm^{-1} (NH stretch) and at 1660–1620 cm^{-1} (C=O stretch) can be used to distinguish between α- and β-chitin (see, for example, Walton & Blackwell (1973); Gow *et al.* (1987)). In nature, chitin is usually deacetylated to some extent and varies in its degree of crystallinity. Most chitin samples will give two bands in the 1660–1620 cm^{-1} region, namely 1656 cm^{-1} and 1626 cm^{-1}. The exception to this is chitin found in the spines of the diatom *Thalassiosira fluviatilis*, which gives rise to only one sharp band at 1626 cm^{-1} (Muzzarelli 1973). The finding that this type of chitin is highly crystalline had led Muzzarelli to postulate that the band at 1626 cm^{-1} represents a coupled vibration of the unit cell, whereas that at 1656 cm^{-1} is due to an uncoupled vibration in the less ordered regions of the molecule where the *N*-acetyl groups are missing. The presence of two bands in this region for chiton radula is therefore highly suggestive that this type of chitin is partly deactylated. In this context, it has been estimated that one in every six residues on lobster carapace chitin polymer is deacetylated (Rudall 1963).

Although FT–IR could not distinguish the polymorphic form of radular chitin because of its amorphous nature, XRD readily indicated the α-form. Lowenstam & Weiner (1985) also found α-chitin in the radula of the chiton *Acanthopleura haddoni*, but as the analysis was done on stage 1 segments that had not been deproteinated, the final diffraction pattern obtained could have been affected by protein impurities. The finding that radular chitin exists as the α-form, in which the polymeric chains occur in an antiparallel arrangement, is in common with other chitinoproteic structures such as insect and crustacean cuticle. In nature, α-chitin is the more stable and common polymorph (Gow *et al.* 1987). Furthermore, the presence of the α-phase of chitin may be significant in the context of the microarchitecture of the tooth and its overall mechanical properties (Muzzarelli (1977) and references therein).

The positive reaction obtained from the Van Wisselingh staining technique confirms the presence of chitin in stage 1 segments. Because of the harsh treatment necessary to effect the conversion of chitin to the deacetylated polymer chitosan, only materials such as inorganic solids, chitin and cellulose are likely to remain (Tracey 1955). Some confusion exists, however, as to the specificity of both Alcian blue and Hale's colloidal iron stains in the chiton radular system (see, for example, Runham (1963*b*)). In our study, both Alcian blue and Hale's techniques gave rise to positive staining reactions, regardless of whether or not the protein had been removed, indicating that these reagents are not specific for either protein or chitin. Variations in staining intensity were noted after deproteination (stronger for Alcian blue, weaker for Hale's) indicating that each dye has slightly more affinity for the chitin or protein phases, respectively.

Histochemical results obtained after protein removal and blocking of residual aldehyde indicated that *A. hirtosa* radular chitin is PAS-negative. However, when the protein was left intact and suitable blocking agents again used, radular sections were weakly positive, indicating an affinity for the protein component of the system. Alternatively, the alkali treatment could have chemically modified the chitin molecule preventing oxidation with periodic acid and subsequent reaction with Schiff's reagent. However, very dilute alkali was deliberately chosen to effect deproteination so that deacetylation was minimized. These results are in contrast to the study of Runham (1963*b*) who attributed a positive PAS reaction to the presence of chitin in the radula of the chiton *Acanthochitona communis*.

The significance of chitin to the cusp structure became readily apparent as microscopic examination of the organic matrix proceeded. The organic matrix in the anterior region of the cusp was characterized by the presence of thick rope-like fibres running parallel to each other, whereas organic matrix fibres in the posterior region were finer and less ordered. The differences observed in the organization and density of organic fibres is almost certainly related to the occurrence of different mineral phases within the cusp. The distribution of magnetite, lepidocrocite and apatite has been mapped by Lowenstam (1967) in several species of chiton. The leading (posterior) surface is always capped by a layer of black magnetite rarely exceeding 10 μm thick (Kirschvink & Lowenstam 1979). Lepidocrocite forms a thin layer immediately behind the magnetite and extending partway down the anterior surface, whereas the remainder of the tooth cusp is calcified in the form of an apatite mineral. In *A. hirtosa* this is a fluorine-substituted hydroxyapatite ($Ca_5(OH, F)(PO_4)_3$) (Kim *et al.* 1986).

The bulk of the mature tooth cusp thus consists of calcified organic fibres. The location, orientation and organization of the rope-like bundles of chitin fibres in the apatite-containing areas of the cusp suggests that they contribute to the mechanical properties of the tooth by imparting tensile strength and flexibility to the tooth cusp. During the course of the feeding action the posterior surface, capped by a layer of magnetite, strikes the rocky substratum and scrapes away filamentous material (Steneck & Watling 1982). It could

PHILOSOPHICAL TRANSACTIONS OF THE ROYAL SOCIETY B BIOLOGICAL SCIENCES

be postulated that without the rope-like bundles of chitin fibres to absorb the shock as mineral (magnetite) strikes rock, the tooth would be more susceptible to fracture. Birchall (1989) has noted that the organic component in nacre serves a similar function in allowing plastic deformation to occur before material failure. In the chiton tooth, it appears that the primary function of the chitin–apatite phase is to provide a tough but flexible support to the cutting edge of the tooth. Differences in hardness between the leading magnetite layer and the softer anterior region, together with the presence of fibres oriented perpendicular to the posterior surface, has led Bullock (1989) to propose a self-sharpening effect in the tooth as the cusp becomes worn. In addition, we have noted that at least some of the chitin fibres in the cusp extend through the junction zone and into the tooth base, presumably making the tooth more resistant to fracture at the cusp–base interface.

In contrast to the densely packed organic fibres in the anterior region of the cusp, the posterior region contains only sparse fibres and undergoes dramatic changes within the first eight rows. Although the first few cusps are generally fibrous, a gradual transformation occurs in the posterior region as the 'compartment' which will later bear the magnetite develops. This transformation is accompanied by a significant decrease in staining intensity presumably due to both the development of finer fibres in this region, and hardening of the radula by tanning of the protein (Runham 1963*b*). These changes in the posterior region occur well in advance of any mineral deposition; in *A. hirtosa* ferrihydrite first appears at about row 15 (Kim *et al.* 1989). SEM micrographs of fractured fully mineralized teeth confirm the lower density of organic fibres in the magnetite layer when compared to the anterior region of the cusp (figure 6). Similarly, Kim *et al.* (1989) noted that in early mineralizing teeth of *A. hirtosa*, crystal density along the posterior surface near the tip of the tooth was far greater than that along the anterior edge, and that crystal density in the posterior region increased towards the centre of the cusp. Van der Wal *et al.* (1989), in studies of the magnetite-bearing layer in the radula teeth of *Chiton olivaceus*, reported that this layer contained a regular array of elongate units. Structures, which may be related to these, were observed in the present study but only in the anterior region of the tooth cusp (figures 13 and 14).

We note that the magnetite compartment clearly does not extend down the full length of the posterior cusp surface, but ends approximately 30 μm above the junction zone (figures 2 and 3). Further evidence for this comes from the observation of the boundary line of crystallites (presumably lepidocrocite) which borders the magnetite compartment meeting up with the posterior surface approximately 25–30 μm above the junction zone. The persistence of the mineral content in a discrete boundary line, despite acid treatment, suggests differences in the physical and/or chemical affinity of the organic matrix in this area compared with that in the rest of the cusp.

Although chitin fibres have been identified in the tooth cusps of *A. hirtosa* by a variety of techniques, it is likely that these occur in close association with proteinaceous components. Weiner (1986) in a review of five different types of mineralized tissue, has noted that acidic macromolecules are always present. It has been suggested that in molluscan shells, for example, specific sites on acidic proteins act as nucleation centres for mineral formation (Mann 1988 and references therein). Because the mineralization of chiton teeth is a complex system, involving the formation of a mineral-rich magnetite region juxtaposed with a quite distinct matrix-rich apatite region, it is likely that selective mechanisms are involved in the deposition of iron and calcium biominerals within the different sections of the cusp. Work is currently underway, therefore, to investigate the nature of the protein component of the organic matrix in an attempt to understand the complex underlying biochemical processes.

We thank G. Thomson, P. Fallon, T. Robertson, D. A. Clarke, I. Watson, Dr R. Chang and Dr N. Kent for their excellent technical assistance, together with the Australian Research Council and Murdoch University for funding. The award of a Commonwealth Postgraduate Research Award to L. A. Evans is also gratefully acknowledged.

REFERENCES

Barnes, R. D. 1980 *Invertebrate zoology*, 4th edn. Philadelphia: Saunders College.

Bullock, R. C. 1989 Mechanical wear of radular denticle caps of *Acanthopleura granulata* (Gmelin, 1791) (Polyplacophora: Chitonidae). *Am. malacol. Bull.* **7**, 13–19.

Birchall, J. D. 1989 The importance of the study of biominerals to materials technology. In *Biomineralization: chemical and biochemical perspectives* (ed. S. Mann, J. Webb & R. J. P. Williams), pp. 491–509. Weinheim: VCH Verlagsgesellschaft.

Culling, C. F. A. 1974 *Handbook of histopathological and histochemical techniques*, 3rd edn. London: Butterworths.

Darmon, S. E. & Rudall, K. M. 1950 Infra-red and X-ray studies of chitin. *Disc. Faraday Soc.* **9**, 251–260.

Furth, A. J. 1980 *Lipids and polysaccharides in biology*. London: Edward Arnold.

Gow, N. A. R., Gooday, G. W., Russell, J. D. & Wilson, M. J. 1987 Infrared and X-ray diffraction data on chitins of variable structure. *Carbohydrate Res.* **165**, 105–110.

Kim, K.-S., Webb, J., Macey, D. J. & Cohen, D. D. 1986 Compositional changes during biomineralization of the radula of the chiton *Clavarizona hirtosa*. *J. inorg. Biochem.* **28**, 337–345.

Kim, K.-S., Macey, D. J., Webb, J. & Mann, S. 1989 Iron mineralization in the radula teeth of the chiton *Acanthopleura hirtosa*. *Proc. R. Soc. Lond.* B **237**, 335–346.

Kirschvink, J. L. & Lowenstam, H. A. 1979 Mineralization and magnetization of chiton teeth: paleomagnetic, sedimentologic and biological implications of organic magnetite. *Earth planet. Sci. Lett.* **44**, 193–204.

Lowenstam, H. A. 1967 Lepidocrocite, an apatite mineral, and magnetite in teeth of chitons (Polyplacophora). *Science, Wash.* **156**, 1373–1375.

Lowenstam, H. A. & Weiner, S. 1985 Transformation of amorphous calcium phosphate to crystalline dahllite in the radular teeth of chitons. *Science, Wash.* **227**, 51–53.

Mann, S. 1988 Molecular recognition in biomineralization. *Nature, Lond.* **332**, 119–124.

PHILOSOPHICAL TRANSACTIONS OF THE ROYAL SOCIETY B BIOLOGICAL SCIENCES

McManus, J. F. A. 1946 Histological demonstration of mucin after periodic acid. *Nature, Lond.* **158**, 202.

Muzzarelli, R. A. A. 1973 *Natural chelating polymers: alginic acid, chitin and chitosan*. Oxford: Pergamon Press.

Muzzarelli, R. A. A. 1977 *Chitin*. Oxford: Pergamon Press.

Reynolds, E. S. 1963 The use of lead citrate and high pH as an electron-opaque stain in electron microscopy. *J. Cell Biol.* **17**, 208–212.

Richardson, K. C., Jarett, L. & Finke, E. H. 1960 Embedding in epoxy resins for ultrathin sectioning in electron microscopy. *Stain Technol.* **35**, 313–323.

Rudall, K. M. 1963 The chitin/protein complexes of insect cuticles. *Adv. Insect Physiol.* **1**, 257–313.

Runham, N. W. 1963*a* A study of the replacement mechanism of the pulmonate radula. *Q. Jl microsc. Sci.* **104**, 271–277.

Runham, N. W. 1963*b* The histochemistry of the radulas of *Acanthochitona communis*, *Lymnaeae stagnalis*, *Helix pomatia*, *Scaphander lignarius* and *Archidoris pseudoargus*. *Ann. Histochim.* **8**, 433–442.

Skujins, J. J., Potgieter, H. J. & Alexander, M. 1965 Dissolution of fungal cell walls by a streptomycete chitinase and β-(1→3) glucanase. *Archs Biochem. Biophys.* **111**, 358–364.

Steneck, R. S. & Watling, L. 1982 Feeding capabilities and limitation of herbivorous molluscs: a functional group approach. *Mar. Biol.* **68**, 299–319.

Tracey, M. V. 1955 Chitin. In *Modern methods of plant analysis* (ed. K. Paech & M. V. Tracey), vol. 2, pp. 264–274. Berlin: Springer-Verlag.

Van der Wal, P., Videler, J. J., Havinga, P. & Pel, R. 1989 Architecture and chemical composition of the magnetite-bearing layer in the radula teeth of *Chiton olivaceus* (Polyplacophora). In *Origin, evolution and modern aspects of biomineralization in plants and animals* (ed. R. E. Crick), pp. 153–166. New York: Plenum Press.

Walton, A. G. & Blackwell, J. 1973 *Biopolymers*. New York: Academic Press.

Webb, J., Macey, D. J. & Mann, S. 1989 Biomineralization of iron in molluscan teeth. In *Biomineralization: chemical and biochemical perspectives* (ed. S. Mann, J. Webb & R. J. P. Williams), pp. 345–388. Weinheim: VCH Verlagsgesellschaft.

Weiner, S. 1986 Organization of extracellularly mineralized tissues: a comparative study of biological crystal growth. *CRC Rev. Biochem.* **20**, 365–408.

(*Received 30 March 1990; Accepted 26 April 1990*)

PHILOSOPHICAL TRANSACTIONS OF THE ROYAL SOCIETY B BIOLOGICAL SCIENCES

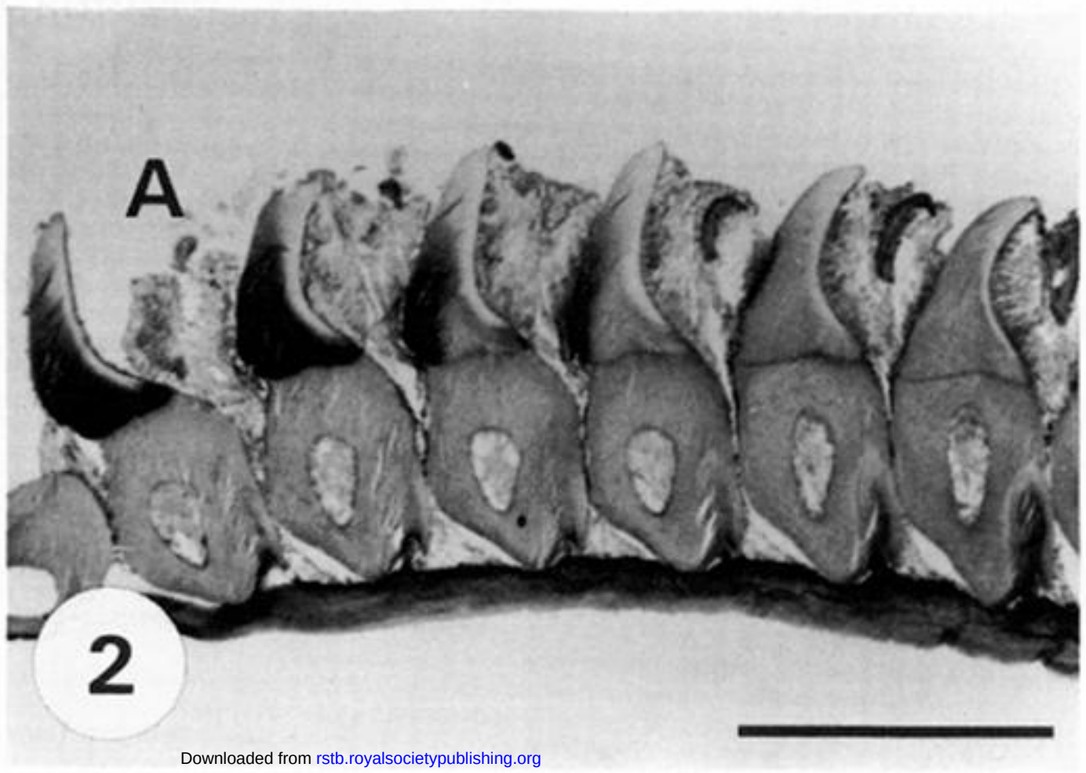

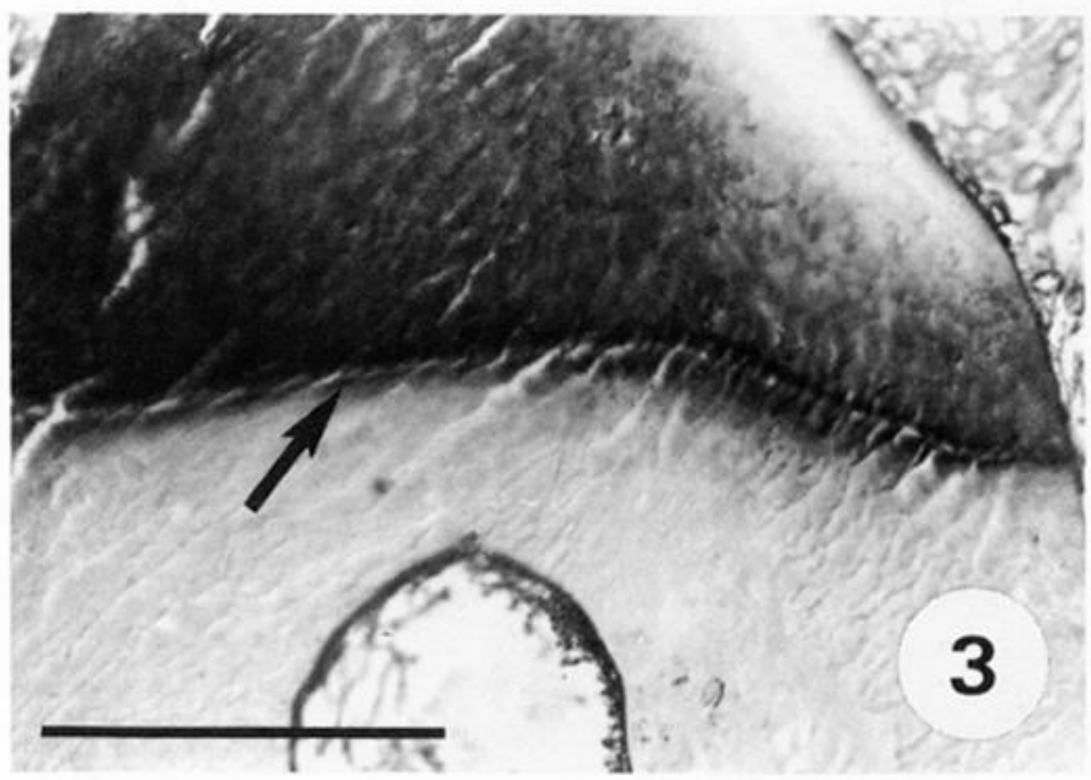

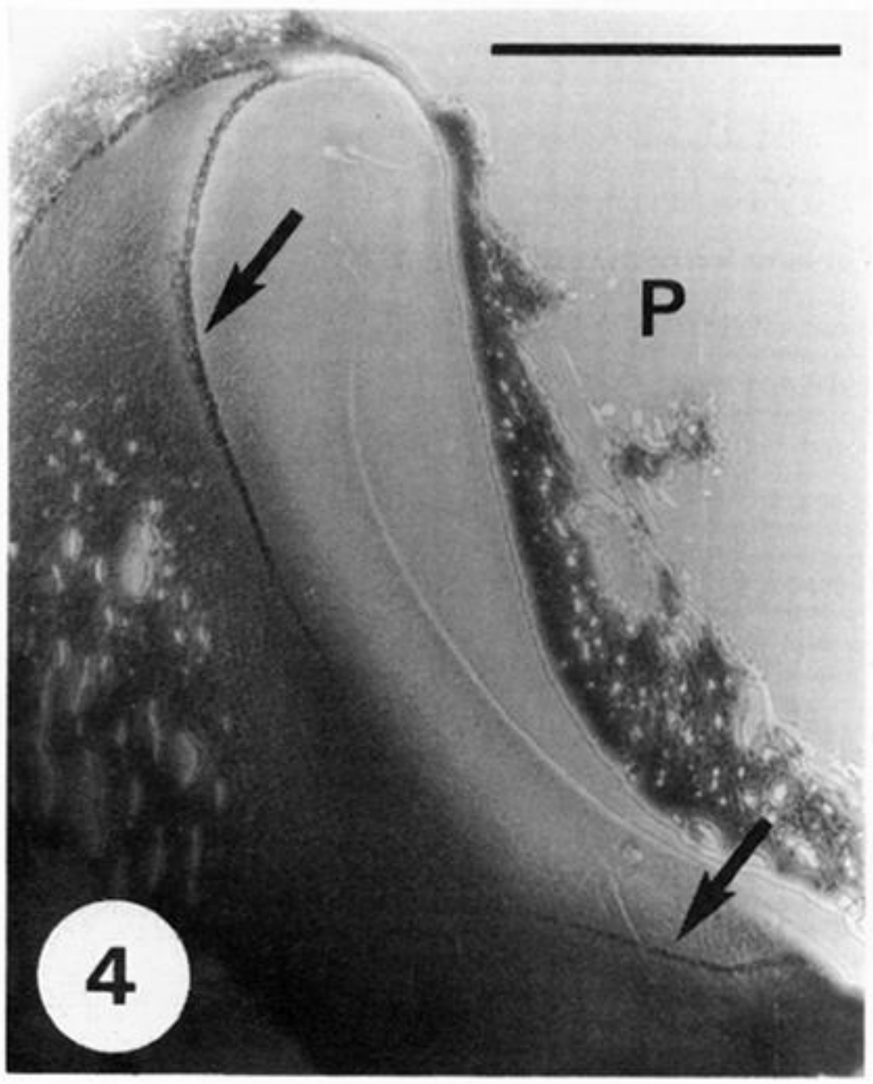

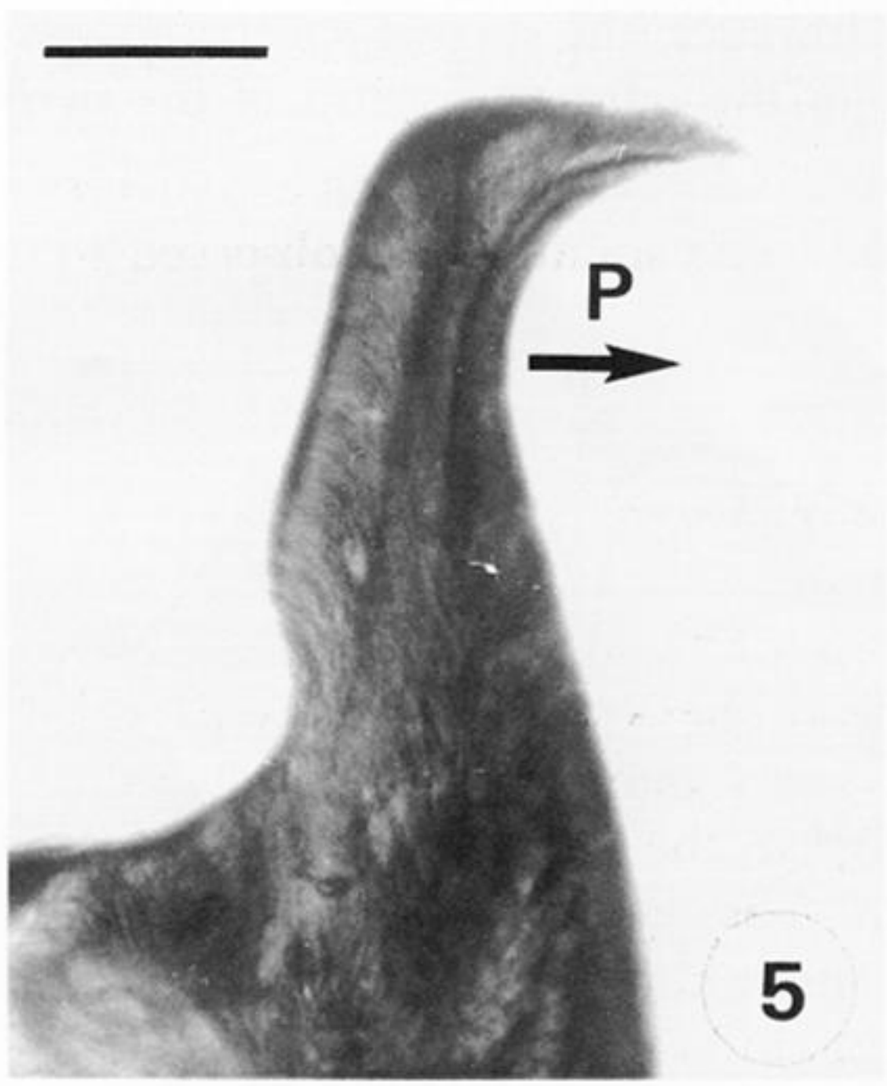

Figure 2. Light micrograph (LM) of longitudinal section through the major lateral teeth following initial tooth formation (stage 1) stained with methylene blue – azure II. Most mature teeth are denoted by A. Scale bar 500 μm.

Figure 3. LM of longitudinal section of major lateral tooth at row 8 showing double-layered junction zone (arrow). Scale bar 50 μm.

Figure 4. LM section of a demineralized mature cusp (stage 4) showing the presence of a line (arrows) delineating anterior and posterior regions of the cusp. P indicates posterior surface of the cusp. Stained with Toluidine blue. Scale bar 100 μm.

Figure 5. LM section of an immature tooth cusp (stage 1) stained using Van Wisselingh's technique for chitosan and revealing the presence of a dense network of fibres. P indicates posterior surface of the cusp. Scale bar 50 μm.

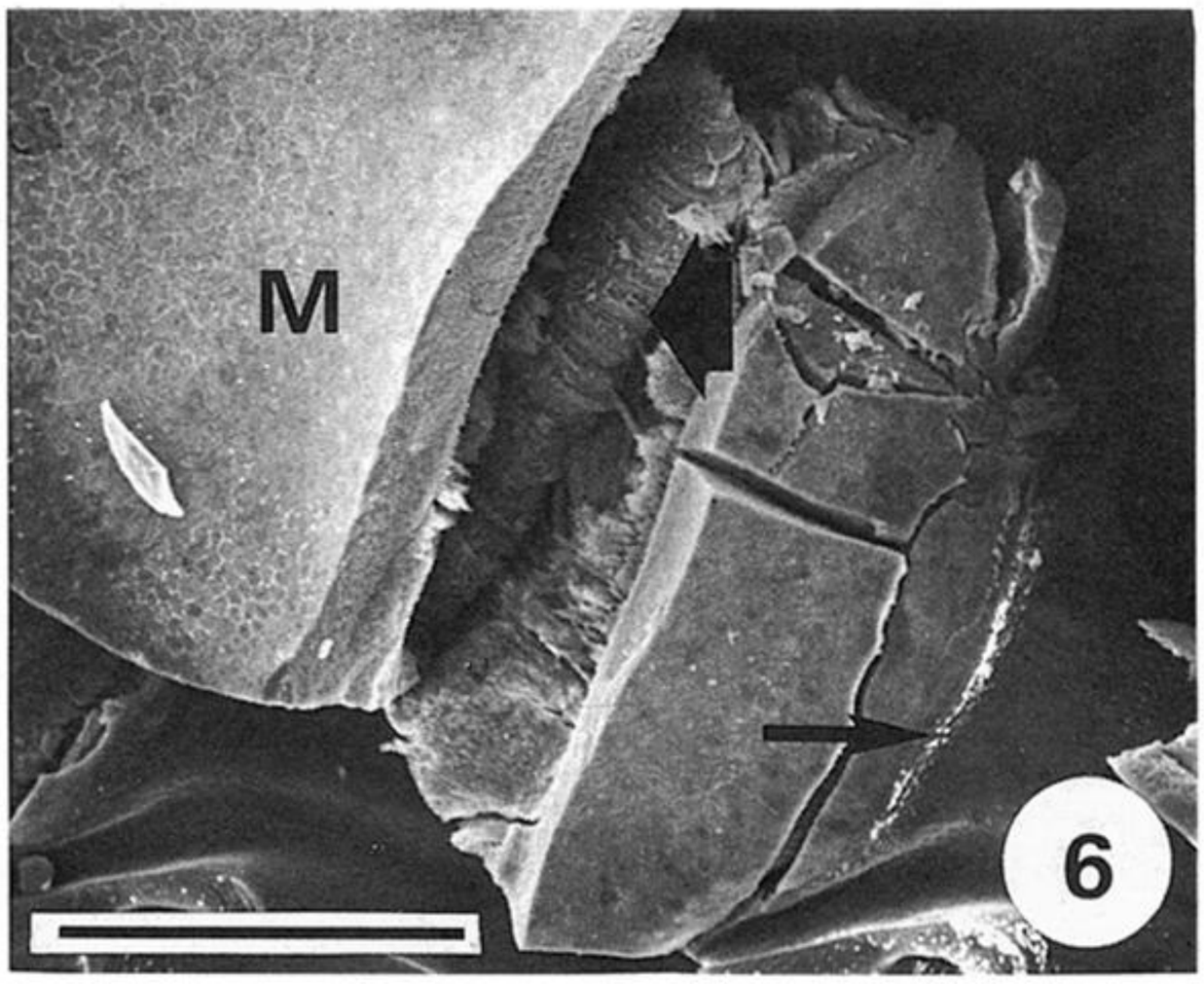

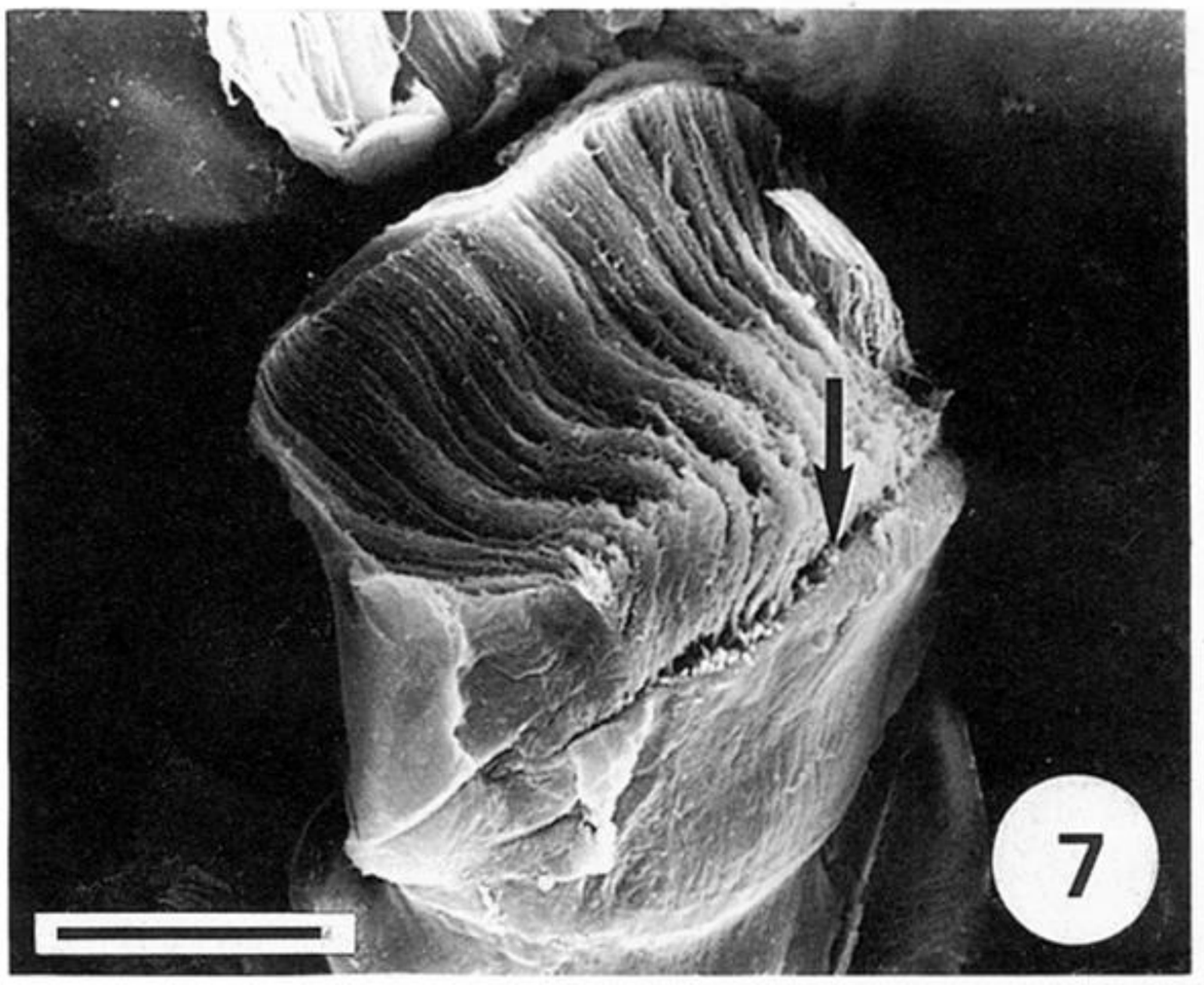

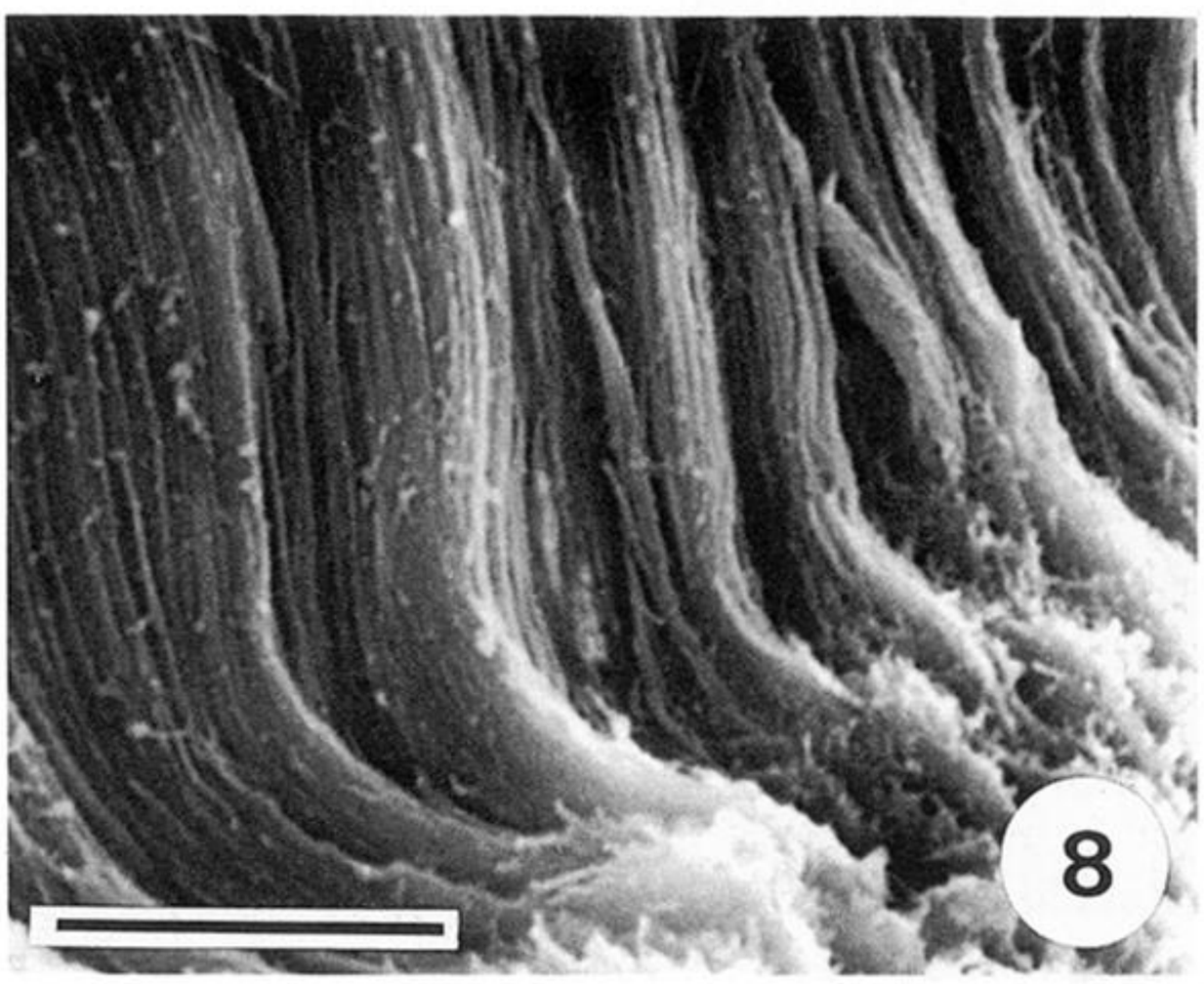

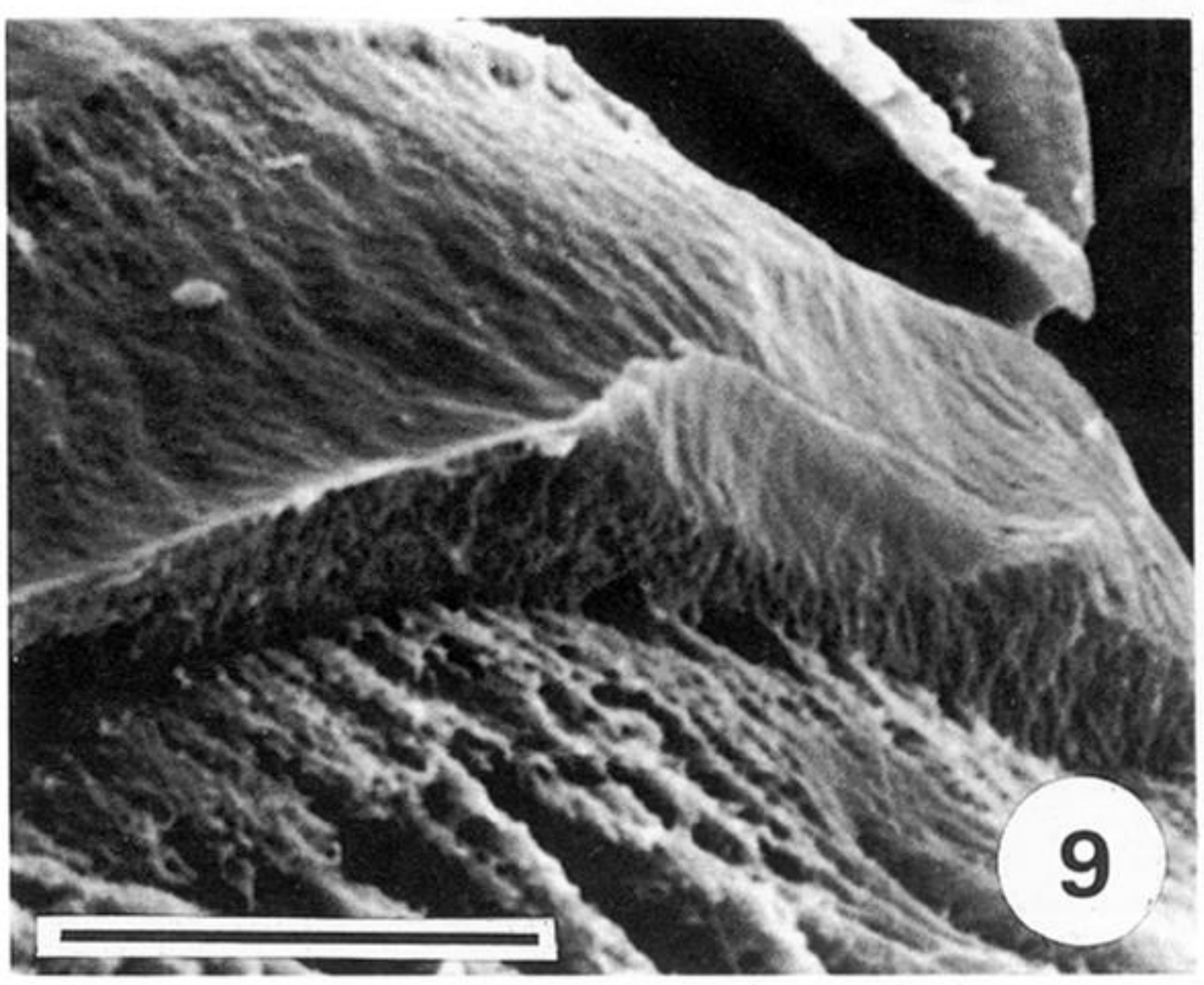

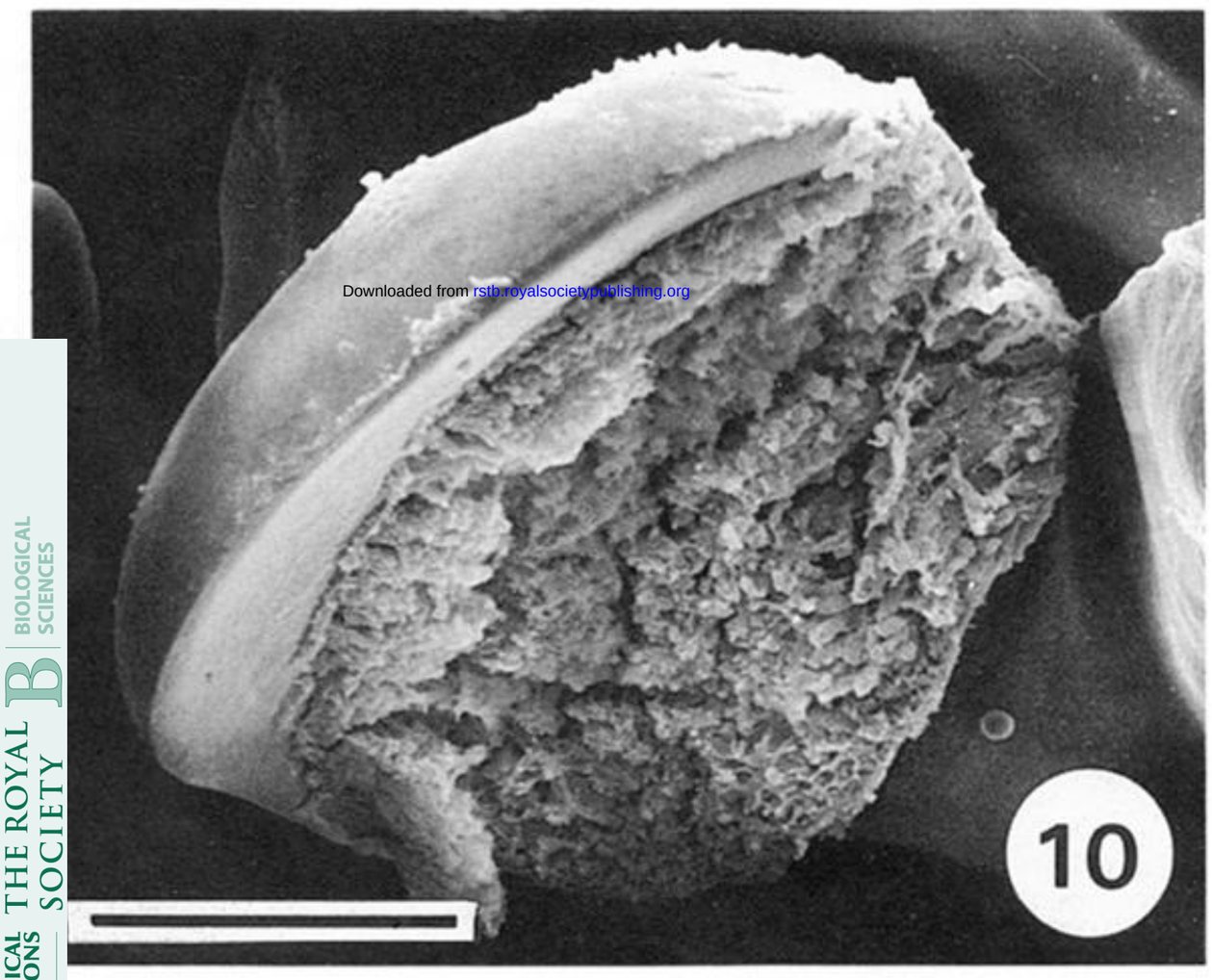

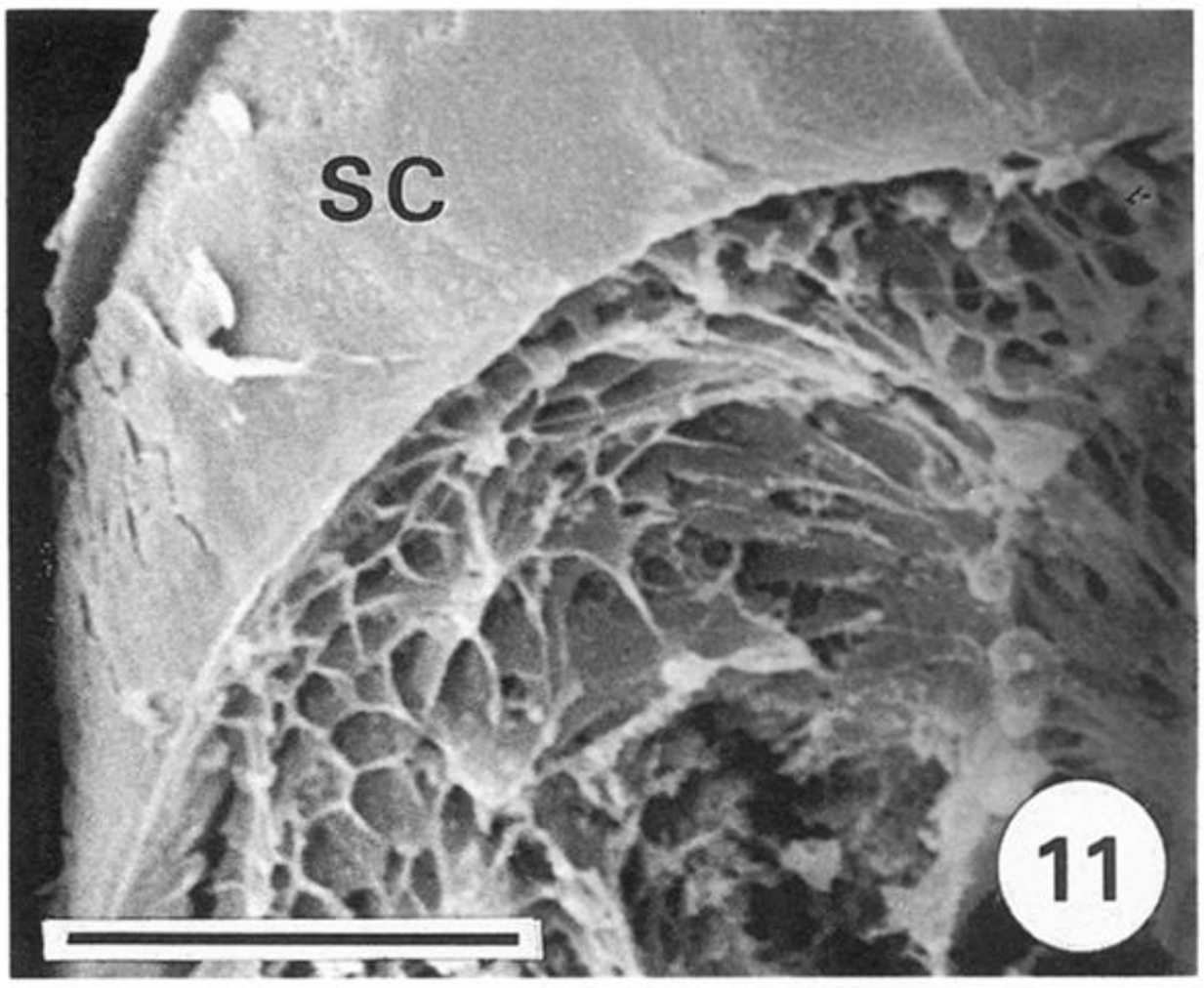

gure 6. SEM of the posterior surface of a fractured fully mature (stage 4) tooth revealing the presence of a discrete ineral layer, presumably magnetite (M) in front of densely packed vertical fibres (broad arrow). The junction zone hin arrow) is also visible well below the major fracture line. Scale bar 100 μm.

gure 7. SEM of an alkali-cleaned acid-etched tooth cusp viewed from the posterior surface showing the presence of rtical rope-like strands of material, presumably chitin. Note, all of the posterior region of the cusp together with irts of the anterior region have been removed during processing. A prominent discontinuity is apparent on the sterior surface (arrow) above the junction zone. Scale bar 50 μm.

gure 8. Higher-powered SEM of the same tooth as in figure 7 showing the detailed structure of the rope-like strands chitin. Scale bar 25 μm.

gure 9. SEM of the horizontal discontinuity frequently observed in alkali-cleaned acid-etched teeth corresponding that arrowed in figure 7. Scale bar 25 μm.

gure 10. SEM of the posterior surface of a hypochlorite-cleaned acid-etched tooth showing removal of only the surface yers. Scale bar 100 μm.

gure 11. SEM of a hypochlorite-cleaned and more deeply acid-etched tooth showing the presence of polygonal bules beneath the posterior tooth surface. Note surface covering (SC) still remains near the tip of the cusp. Scale ır 25 μm.

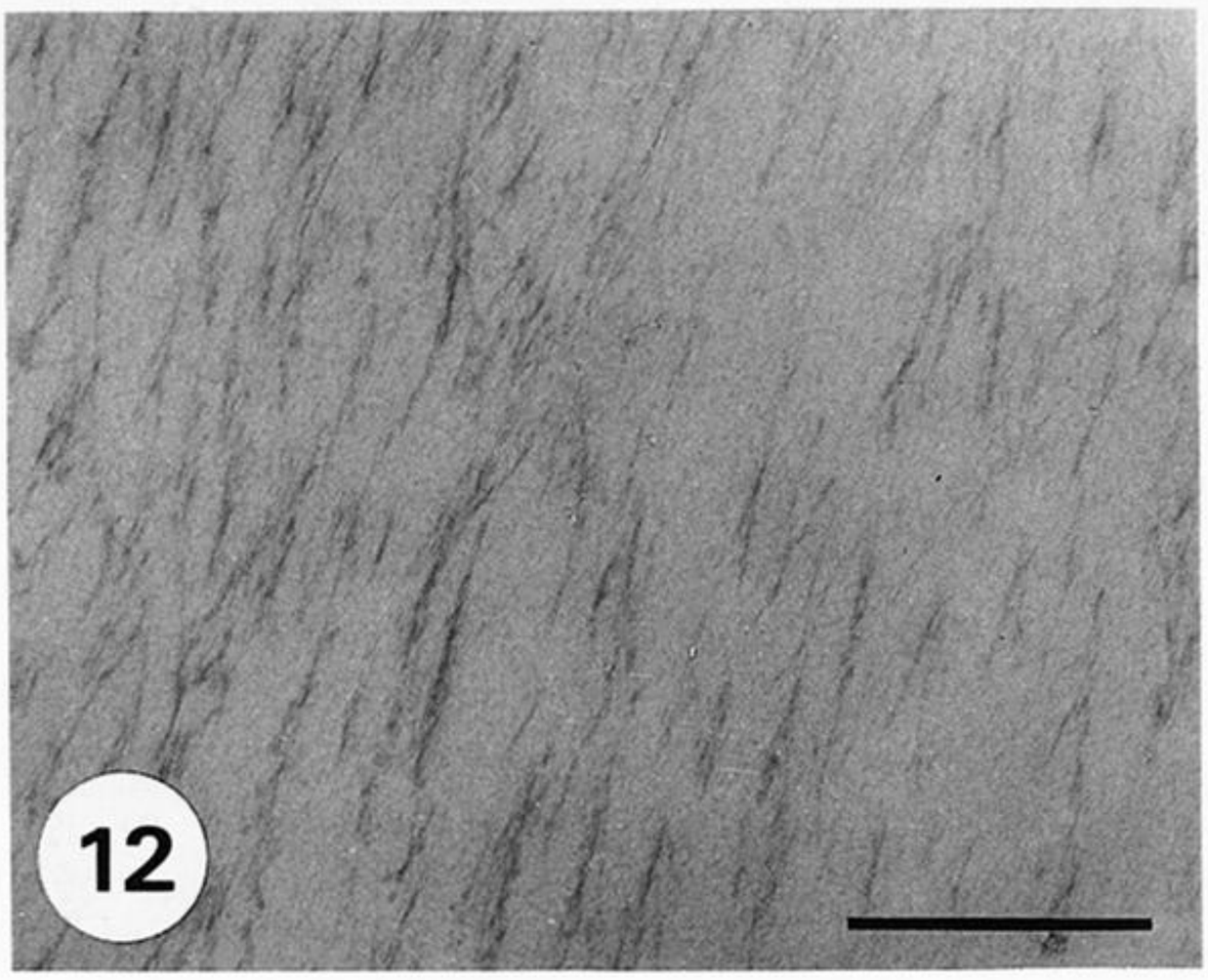

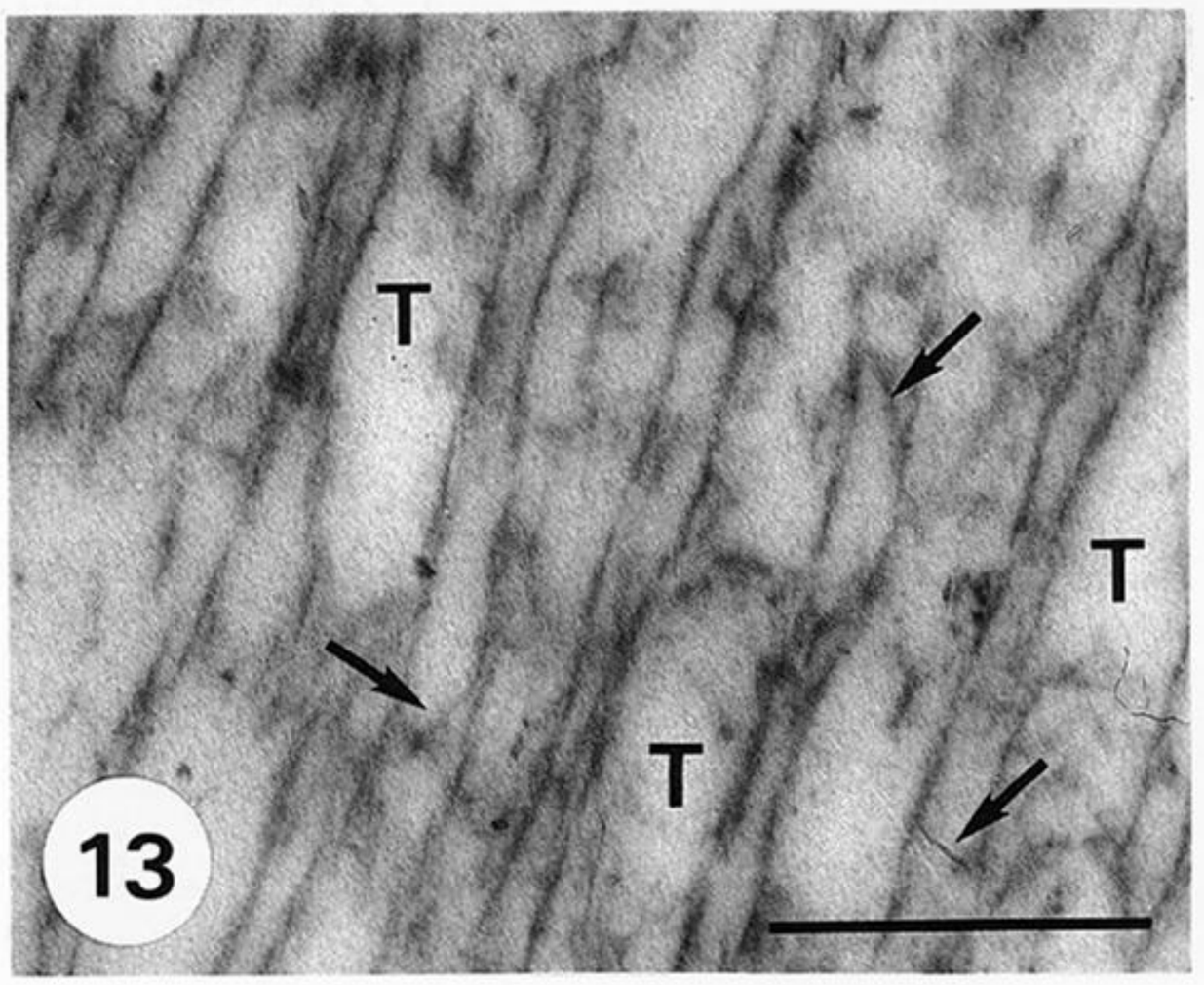

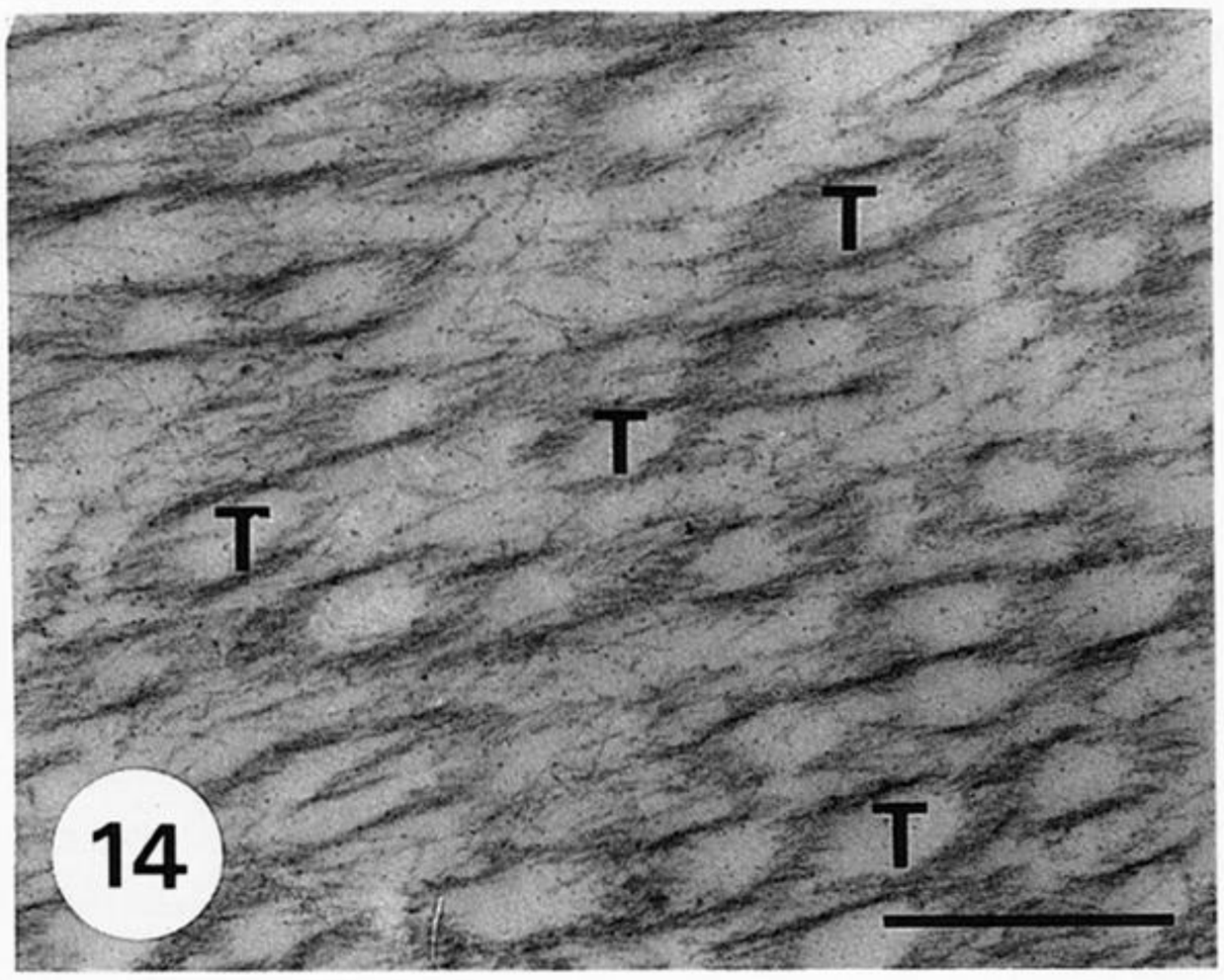

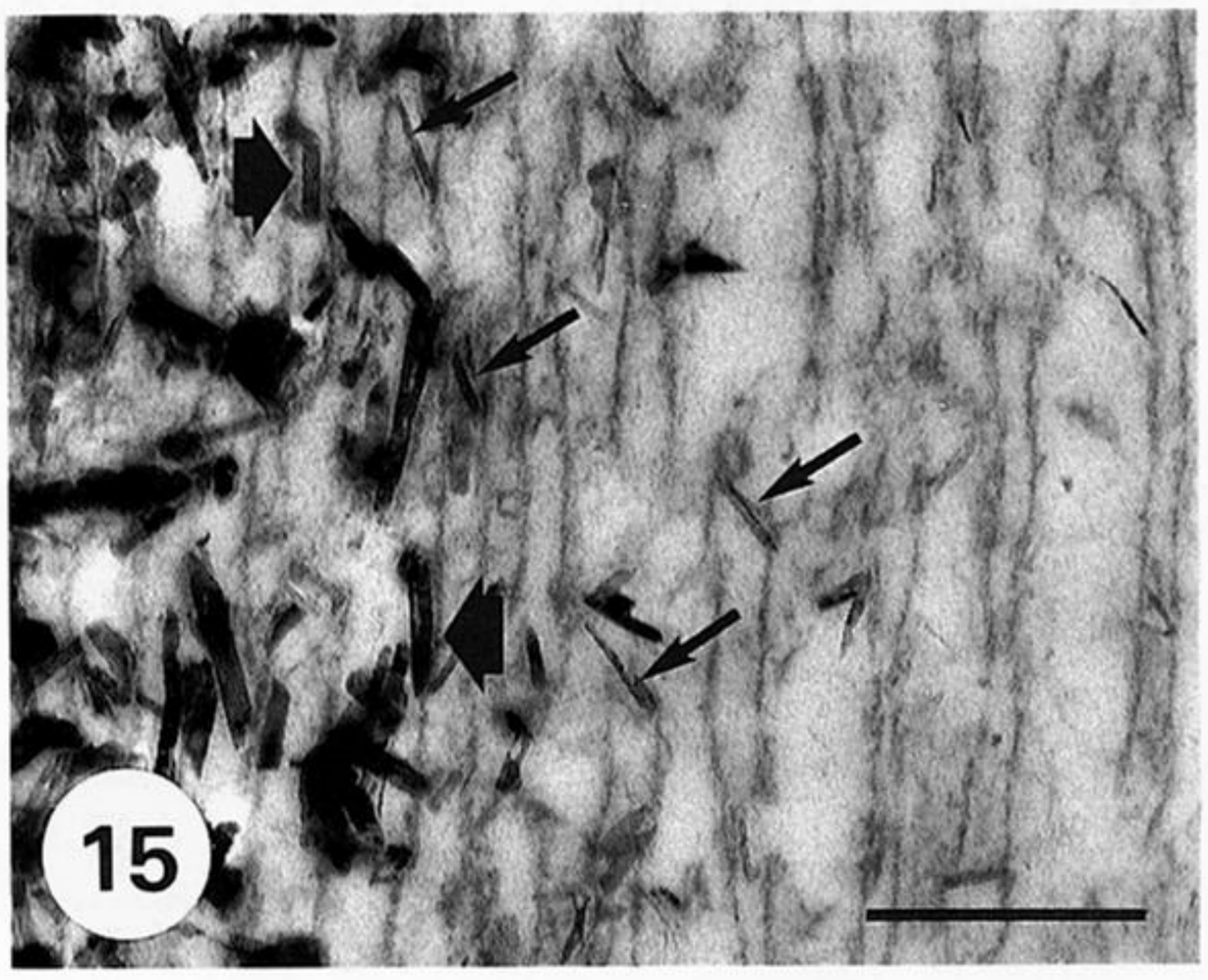

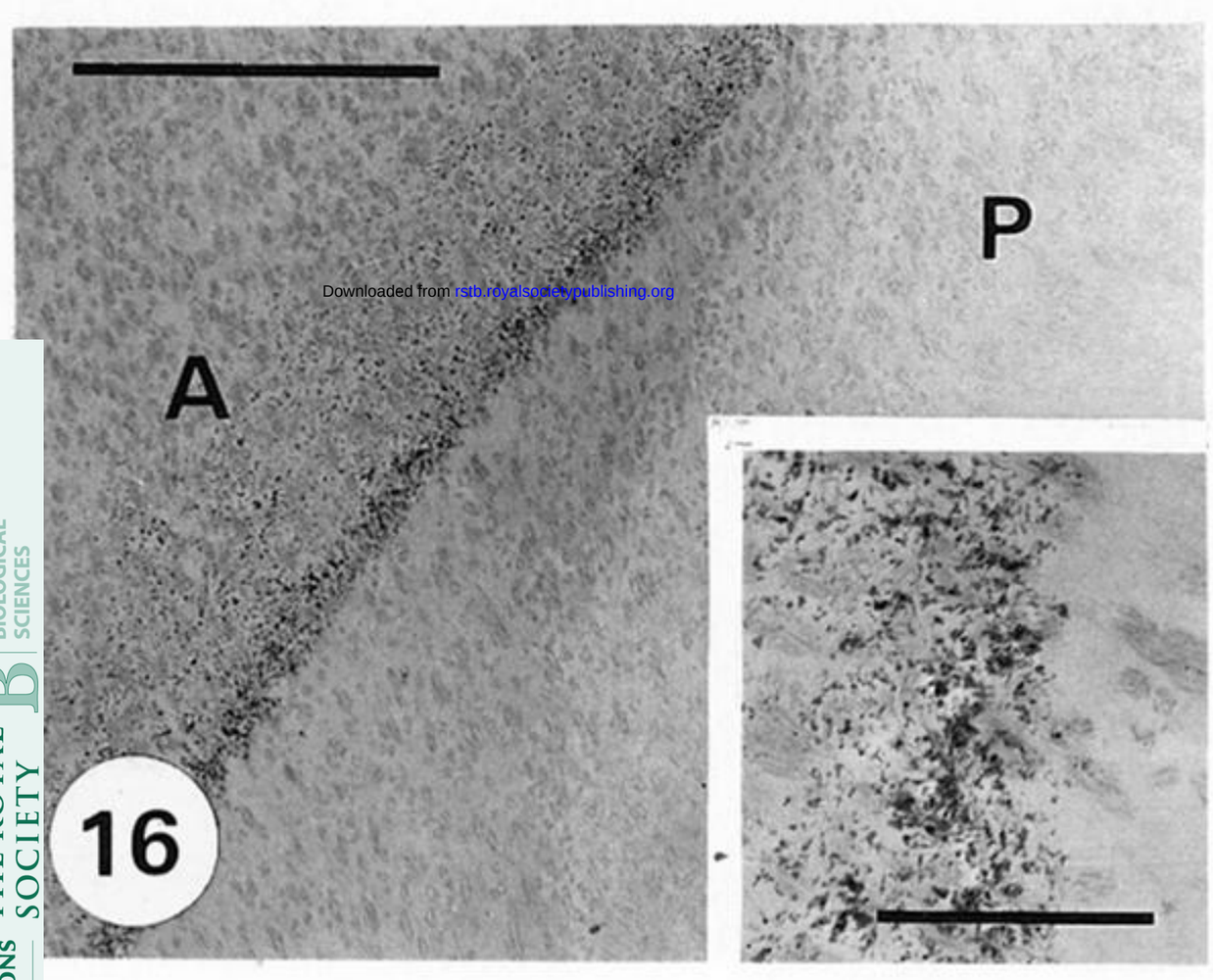

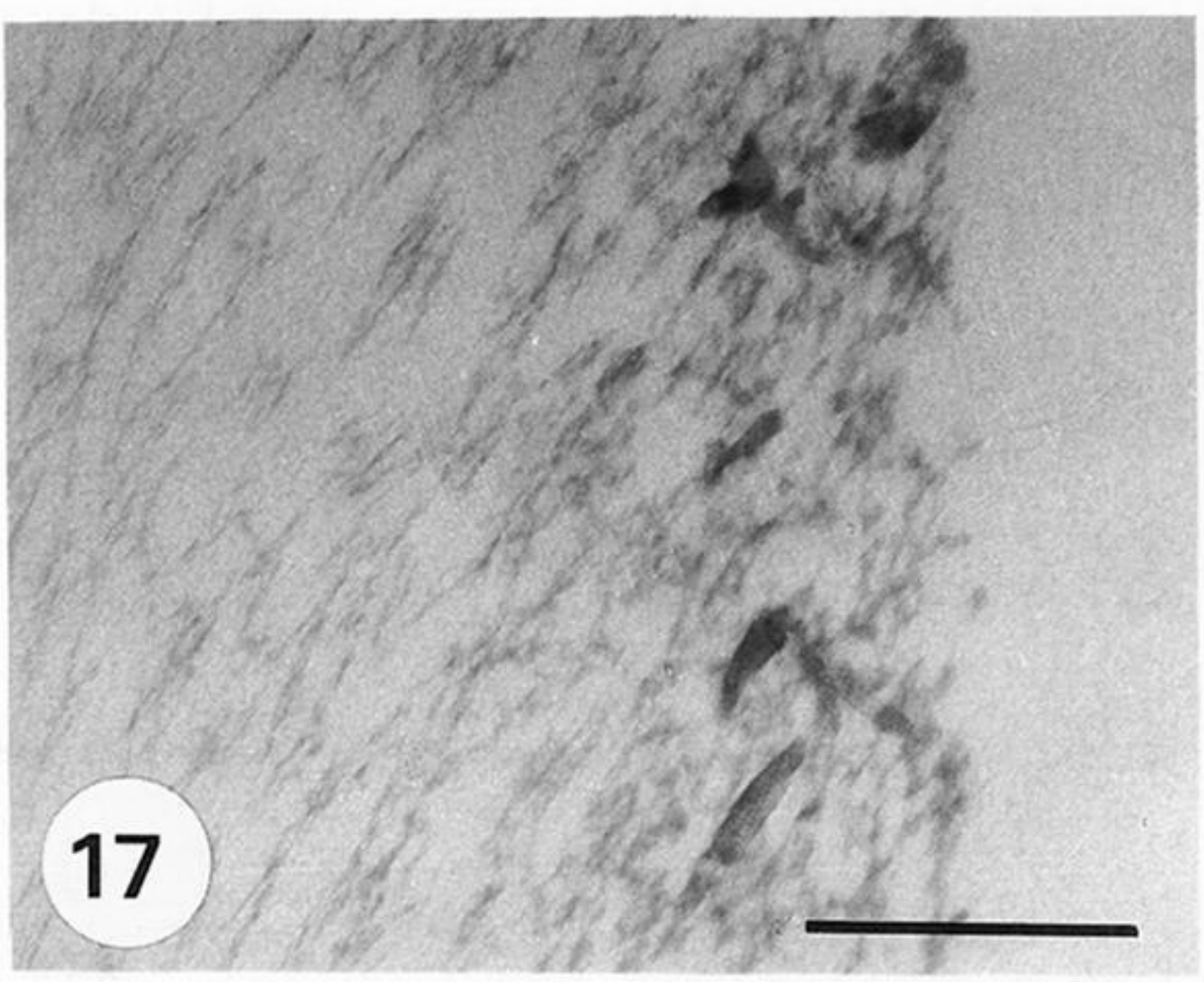

Figure 12. TEM of a stained section of an area of the organic matrix in the posterior region of an acid-treated (stage) tooth cusp showing the presence of sparse fibres. Scale bar 0.5 μm.

Figure 13. TEM of a stained longitudinal section of the anterior region of an acid-treated tooth cusp showing the resence of highly organized fibres arranged as hollow tubules. In some cases cross-links (arrows) can be seen between ıe tubules (T). Scale bar 0.5 μm.

Figure 14. TEM of a stained transverse section of a similar area to that shown in figure 13. The hollow tubules are now pparent as interconnected open rings (T). Note the contrast in fibre density between figure 12 (posterior region) and gures 13 and 14 (anterior region). Scale bar 0.5 μm.

Figure 15. TEM of a stained longitudinal section of the anterior region of an acid-treated mature tooth near the surface. n this region some mineral crystals still remain oriented both parallel to the long axis of the tubules (broad arrows) nd along the interconnecting fibrous bridges (fine arrows). Scale bar 0.5 μm.

Figure 16. TEM of a stained section of the junction between the posterior (P) and anterior (A) regions of an acid-treated ıature cusp showing a diffuse line of crystallites along the boundary line. Scale bar 10 μm. Inset: higher-power TEM f boundary crystallites. Scale bar 2 μm.

Figure 17. TEM of a stained section of the posterior cusp surface of an acid-treated mature cusp showing the more ɔmplex orientation of the fibres at the surface together with the presence of a few crystals. Scale bar 0.5 μm.